Geophys. J. Int. (1991) **106**, 677–694

A parametrized solid earth tide model and ocean tide loading effects for global geodetic baseline measurements

H.-G. Scherneck

Uppsala University, Department of Geophysics, Planetary Geophysics and Geodesy, Hällby, S-755 92 Uppsala, Sweden

Accepted 1991 April 12. Received 1991 March 4; in original form 1990 September 14

SUMMARY

An observation model for earth tide displacements in application to Very Long Baseline Interferometry and similar precise geodetic techniques is developed. It incorporates effects from anelasticity, ellipsoidal figure, and fluid core resonance. Based on a harmonic development of the external potential, the model follows the familiar Love number concept. The transfer function of the earth to each harmonic is formulated in terms of coupled harmonics in the space domain and fulfils the causality condition in the time domain. Solve-for parameters can be chosen flexibly. The guideline, however, has been to provide a minimum set of well-defined and well-resolvable tide response parameters for analysis of observations. The aim of accuracy for tide displacements prediction is below 1 mm.

Being the major perturbation of the solid earth tide, ocean tide loading effects are computed, and the accuracy of the models involved is discussed. It appears that the major error source relates to those ocean tide frequencies for which global models are not available. These frequencies form a continuum with a power spectrum being largely a result of non-linear tide interaction. The associated loading effects cannot be reliably interpolated from global tide models, which are available only for a few distinct frequencies and which disregard tidal intermodulation. Thus, an accuracy of 1 mm for computed loading tide displacements cannot always be achieved.

Key words: earth and ocean tides, precise geodetic measurements, surface displacements.

1 INTRODUCTION

Very Long Baseline Interferometry (VLBI) and Satellite Laser Ranging (SLR) techniques have demonstrated their capability to determine a number of geodynamic parameters of the earth. Besides the monitoring of changes of baselines within global networks, the quantities which relate to precession, nutation, polar motion, Universal Time variations, and tidal deformation can be resolved. This report will focus on the tide displacement problem and discuss it in application to VLBI, but can easily be interpreted also from the SLR point of view.

What makes VLBI an attractive measurement technique in geophysics and geodesy is its tie to fundamental physical constants and the quasi-inertial reference frame to which it relates (Coates *et al.* 1985; Carter & Robertson 1985; Dickey & Eubanks 1985). VLBI data analysis compares observations of radio wave delays with those predicted on the basis of an earth model that comprises many individual contributions to baseline vector changes due to earth dynamics (Herring 1986). The solid earth, the liquid core and the oceans are represented by six submodels, two of which compute and solve station displacements related to tides: solid earth and ocean loading tides.

This report gives an account of the tide displacement problem. Its aim is to summarize the results of mainly the recent decade's efforts in studies of the earth's response to the tide potential and to the surface loads exerted by the ocean tides. The results are compiled in a comprehensive and conveniently formulated displacement model for application in VLBI analysis software. Most tide effects involved are discussed in detail. Especially where controversies exist in the literature, this paper attempts to sort out the arguments and conclude a feasible approach.

Demands for a revision of the surface displacements model arise, recognizing the increase of precision of VLBI as a product of ongoing development of the techniques and analysis procedures involved. Apart from the application of a tide model for the determination of tide related quantities within VLBI, propagation of errors from a tide predicting model into other solved-for parameters must be avoided.

Recent work using recording gravimeters shows that solid

earth tide predictions can be verified at the one part per thousand level—ocean tide loading being the largest perturbation—provided the instruments have been carefully calibrated (Baker, Edge & Jeffries 1989). In this respect, calibration presents no problem in VLBI. However, the earth's response to the tidal potential constitutes the entire tide variation seen by the (geometric) method VLBI, whereas gravity effects consist of 85 per cent direct effect from the tide raising bodies and only 15 per cent earth response. It is the earth's response which involves more complicated and therefore more uncertain models. The signal-to-noise ratios of both techniques are on the other hand 80 dB (gravity) respectively 50 dB (VLBI). Thus, a 1 mm accuracy demand on a solid earth tide displacement model appears reasonable, and 1 mm error is acceptable as a single-source contribution to the total error budget.

The currently used tide model aims at an accuracy of 5 mm. Apart from being dissatisfied with this figure in comparison with current standards, the formulation is found to be too simplistic to be improvable by a few amendments. A more rigorous approach will be presented, which at the same time is flexible to successively incorporate or support additional geodynamic processes relevant for VLBI.

Solutions of tide parameters have been presented by—among others—Carter, Robertson & MacKay (1985), Herring *et al.* (1983), and Sovers *et al.* (1981). Fully three-component ocean tide loading effects have only recently been incorporated (Schuh 1987). The ocean loading effects are on the order of centimetres, horizontal components being roughly one third of the vertical displacement (Scherneck 1983, 1987). In order to avoid that ocean loading perturbations are absorbed in (station-dependent) solid earth tide parameters, their effect needs to be subtracted from the radio wave delays subjected to analysis. Recently, Schuh & Möhlmann (1989) demonstrated that this indeed lowers the post-fit residual.

It is hoped that the tide model presented leads to tide parameters solutions with a greater degree of global consistency, so that regional anomalies of tidal movements can be assessed and results be used more safely in investigations of lateral heterogeneities of the earth.

Two terms frequently used in this report require introduction: the term 'tide component' characterizes the type of observation, which are surface displacements, gravity perturbations, etc. The terms 'tide constituent' and 'partial tide' are applied to a single tide wave, i.e. the single sinusoid with which a particular spherical harmonic component of the tide raising potential in space varies in time. Frequently used abbreviations and some symbols are given in Table 1.

2 SOLID EARTH TIDE DISPLACEMENTS

2.1 Objectives for a parametrized model

The guidelines for the formulation of observation equations for solid earth tide displacements were set by the following demands.

(a) The response parameters have a straight-forward and consistent relationship with the physics of the problem.

(b) The set of parameters resolvable in experiments is flexible and able to reduce to a small set of key parameters.

(c) The parametrization is independent of the time and frequency domain properties of the observation method.

(d) As many parameters as possible provide cross-reference, i.e. they are relevant to other submodels of the full set of observation equations.

The resolving power of the method shall determine which parameters are suitable for analysis; thus, different instrument and analysis configurations can contribute to the same basic model. The main objective of this report is to point out the important earth tide parameters and make them available for estimation in dedicated experiments. The two geophysically most relevant phenomena are the viscoelastic response of the earth and the nearly diurnal resonance of the liquid core. Perturbation of the tide response due to the flattening of the earth is carefully considered.

In addition, tide predictions from a set of standard parameters have to achieve submillimetre accuracies in order to improve currently used methods (IERS-Standards, McCarthy 1989; MASTERFIT VLBI-software, Fanselow & Sovers 1985; CALC/SOLV, Ma 1978).

The formulation emphasizes the following basic principles: compatibility with the principle of causality; proper separation of space and time related effects; definition and use of base-function and reference systems as simply and clearly as possible. Parametrized, continuous formulations are the preferred means to characterize the tidal earth rather than numerical tables.

The proposed tide model is based on harmonic tide potential development. This provides from the start the proper expansion in terms of spherical harmonics (SH) required to compute tides of an elliptical body along the mainstream of theories.

Utilization of harmonic tide development in application to VLBI has originally been suggested by Büllesfeld & Schuh (1986), emphasizing the improvements in accuracy achieved by Büllesfeld (1985) as compared to the standard potential by Cartwright & Tayler (1971) and Cartwright & Edden (1973). Adoption of a new standard is under progress at the

Table 1. Abbreviations and symbols.

Abbreviations and symbols

SH	- Spherical harmonics
NDR	- Nearly Diurnal Resonance
$P_n^m(x)$	- conventional associated Legendre polynomials, $\int (P_n^m)^2 dx = 2(n+m)!/(n-m)!/(2n+1)$
φ, λ	- exclusively denoting geocentric colatitude and longitude
ι	- (greek iota) a Love number from the set {h, l (, k)}
S_{sa}, M_m, M_f, K_1, O_1, P_1, Q_1, M_2, S_2, N_2, K_2, L_2, M_0S_0	- Darwin's tide symbols, c.f. Melchior (1978, pp.10-34)

Subscripts:

bt	- body tide (= solid earth tide)
ot	- ocean (loading) tide
LL	- associated with Load Love number
cal	- associated with calibration
j	- exclusively used to numerate tidal constituents

Commission on Earth Tides under the International Union of Geodesy and Geophysics (IUGG) (Friedrich & Zimmermann 1989), considering recent work by Tamura (1987) and Xi (1987).

Basing the tide response model on a frequency spectrum of the tide potential has the main advantage that the models for core resonance and the viscoelastic response can be parametrized in the frequency domain. Constraints of the model as to comply with causality can then be derived with the Hilbert transform (*cf.* Dehant & Zschau 1989).

2.1.1 Reference system

The adopted coordinate system for tide potential and displacement is the spherical equatorial system used by Wahr (1981). Dimensionless response parameters, the generalized Love numbers, are derived using suitable scaling constants like earth radius and normal gravity, the role of which is conventional rather than physical.

The response of the ellipsoidal earth is characterized in this system as a coupled set of base functions (spherical harmonics), excited by a single base function; the amplitude coefficients of the displacements harmonics relate to the amplitude of the external tide harmonic. This system is in some sense contrary to that of Dehant (1987) that sets the local values of excitation and response into proportion, with the consequence that latitudinally dependent response functions result, some of which obtain singularities. This is avoided here.

Moreover, the geocentric coordinate system used in this report is compatible with the reference system of the IERS-Standards. However, care must be taken as regards the global scaling constants (normal gravity and radius) implicit in the theoretical results.

2.2 The observation equations

The following properties of the earth relevant to tides are considered decoupled from each other at the level of 0.1 mm of displacement: mantle rheology and the Nearly Diurnal Resonance (NDR) of the core; mantle rheology and coupling of the spherical harmonics of the displacement field. Before the parametrized factorization of the earth response is presented, the model Wahr (1981) is reviewed in order to emphasize an important aspect concerning space and time domain separability.

The lunisolar tide potential is given in the following harmonic expansion:

$$\psi(r, t) = g_e \, \mathcal{R}e \sum_j \Psi_j (r/r_e)^{n_j} P_{n_j}^{m_j} \times (\cos\varphi) \exp[i(\chi_j + \omega_j t + m_j \lambda)], \quad (2.1)$$

where r_e is the equatorial radius and g_e normal gravity at the equator (see also Appendix A). Displacements u at a site on the earth surface, at geocentric colatitude φ and longitude λ, are accordingly described by the coupled set of spheroidal base functions $S_n^m(\varphi, \lambda)$

$$S_n^m(\varphi, \lambda) = \left[P_n^m(\cos\varphi)\mathbf{r} + \partial_\varphi P_n^m \times (\cos\varphi)\boldsymbol{\varphi} + \frac{im}{\sin\varphi} P_n^m(\cos\varphi)\boldsymbol{\lambda} \right] \exp(im\lambda) \quad (2.2)$$

in the form

$$\mathbf{u}(\varphi, \lambda, t) = u_r \mathbf{r} + u_\varphi \boldsymbol{\varphi} + u_\lambda \boldsymbol{\lambda} = \mathcal{R}e \sum_j U_j(\omega_j, \varphi, \lambda) \exp(i\omega_j t), \qquad \omega_j > 0, \quad (2.3a)$$

with the displacement spectrum

$$U_j(\omega, \varphi, \lambda) = \left[\mathcal{L}_{nm}(\omega) S_n^m(\varphi, \lambda) + \sum_{kl} \mathcal{C}_{nmkl}(\omega) S_k^l(\varphi, \lambda) \right] \Gamma_j \quad (2.3b)$$

where $\Gamma_j = \Psi_j \exp(i\chi_j)$ are the coefficients of a harmonic tide development (spectrum) in metres, $\omega = \omega_j$, $\chi = \chi_j$, $n = n_j$ and $m = m_j$. The static tide must be eliminated to comply with IERS-Standards. The harmonic response is represented by a diagonal matrix of frequency dependent Love numbers $\mathcal{L}_{nm}$ representing the spherical case. The remaining terms are ellipsoidal perturbations, 3×3 coupling matrices $\mathcal{C}_{nmkl}$ with non-zero elements according to the selection rules of Wigner's $3j$-symbols. Wahr found short expressions for (2.3b) when he preserved the product $P_2 P_n^m$ rather than using the expansion in terms of a series of P_k^m. With only a few non-zero coupling coefficients,

$$U_j(\omega, \lambda) = \left[\mathcal{L}_{nm}(\omega) S_n^m(\varphi, \lambda) + \bar{\mathcal{C}}_{nm}(\omega) \bar{S}_n^m(\varphi, \lambda) + \sum_{kl} \bar{\mathcal{C}}_{nmkl}(\omega) S_k^l(\varphi, \lambda) \right] \Gamma_j,$$

$$\bar{S}_2^m(\varphi, \lambda) = P_2(\cos\varphi) S_2^m(\varphi, \lambda).$$

To first order in perturbation (in Wahr's system of unit normalized SH) these are

$$\mathcal{L}_{nm} = \mathrm{diag}(h_{nm}, l_{nm}, l_{nm}),$$

$$\bar{\mathcal{C}}_{nm} \cong 0 \quad \forall n \neq 2, \qquad \bar{\mathcal{C}}_{2m} = \mathrm{diag}(h_{2m} y_m, l_{2m} z_m, l_{2m} z_m),$$

$$\bar{\mathcal{C}}_{nmkl} \cong 0 \quad \forall n \neq 2, \qquad \tilde{\mathcal{C}}_{2m4m} = \mathrm{diag}(0, l_{2m} l_{+m}, l_{2m} l_{+m}),$$

$$\bar{\mathcal{C}}_{nmnm} = 0 \quad \forall n, m, \; m > 0, \qquad \tilde{\mathcal{C}}_{pq}^{2m9m} = i l_{2m} w_{+m} (\delta_{3p}\delta_{2q} - \delta_{2p}\delta_{3q}),$$

$$\bar{\mathcal{C}}_{2m2l} = 0 \quad \forall l \neq m, \; 1 \leq q \leq 3, \qquad \text{with} \quad \bar{\mathcal{C}}_{nmkl} = (\bar{c}_{pq}^{nmkl}), \quad 1 \leq p \leq 3,$$

So far, the scheme separates time- (frequency) and space- (SH degree and order) dependent properties in a system of harmonic base functions.

The coupling coefficients y, z, l_+ and w_+ are of the order of the flattening of the earth when compared to the Love numbers h and l. This enables the elimination of common factors for the NDR of the core and for the viscoelastic relaxation of the mantle. The NDR appears only in the case of diurnal tides, $(n, m) = (2, 1)$, and is confined to a narrow band of frequencies. Thus, effects of mantle rheology on the resonance are practically frequency independent. Possible dependence of viscoelastic relaxation on SH order m can be neglected (Wang 1990, personal communication).

Instead of scaling the resonant coefficients z_1, l_{+1} and w_{+1} with respect to the resonant l_{21}, the NDR effect as well as the other response terms scaled with respect to two real valued, frequency-independent basic Love numbers H and L. The following observation equation results:

$$U_r = H \beta_{nm}^{(h)} V_n^{(h)}(\omega)[1 + \delta_{n2}\sigma_{m1} C_{\mathrm{NDR}}^{(h)}(\omega)] \times (1 + y_m \delta_{n2} P_n^0) P_n^m \Gamma_j e^{im\lambda},$$

$$U_\varphi = L\beta_{nm}^{(l)} V_n^{(l)}(\omega)\Big\{\partial_\varphi P_n^m + \delta_{n2}\Big(zP_2\,\partial_\varphi P_2^m + l_m^+\,\partial_\varphi P_4^m + w_m^+ \frac{mP_3^m}{\sin\varphi}\Big) + \delta_{n2}\delta_{m1} C_{\mathrm{NDR}}^{(l)}(\omega)\Big[(1+\bar{z}P_2)\,\partial_\varphi P_2^1 + \bar{l}^+\,\partial_\varphi P_4^1 + \bar{w}^+ \frac{P_3^1}{\sin\varphi}\Big]\Big\}\Gamma_j e^{im\lambda},$$

$$U_\lambda = L\beta_{nm}^{(l)} V_n^{(l)}\Big\{\frac{mP_n^m}{\sin\varphi} + \delta_{n2}\Big(zP_2\frac{mP_2^m}{\sin\varphi} + l_m^+\frac{mP_4^m}{\sin\varphi} + w_m^+\,\partial_\varphi P_3^m\Big) + \delta_{n2}\delta_{m1} C_{\mathrm{NDR}}^{(l)}(\omega)\Big[(1+\bar{z}P_2)\frac{P_2^1}{\sin\varphi} + \bar{l}^+\frac{P_4^1}{\sin\varphi} + \bar{w}^+\,\partial_\varphi P_3^1\Big]\Big\} i\Gamma_j e^{im\lambda}, \tag{2.4}$$

to be inserted into (2.3). The NDR spectrum is contained in C_{NDR}, the viscoelastic relaxation spectrum in V_n. The β's denote Love number ratios for different order and degree of SH. Setting $\beta_{21}^{(h)} = \beta_{21}^{(l)} = 1$, $H = |h_{21}(O_1)|$ and $L = |l_{21}(O_1)|$ pivots the model on the O_1 tide. First-order deviations of β_{20} and β_{22} from unity are proportional to the flattening parameter. The higher degree β_{nm} are uncritical and can be adopted from e.g. Farrell (1972), neglecting their dependence on m. Table A2 (Appendix A) specifies numerical values for use with conventional associated Legendre polynomials $P_n^m(\cos\varphi)$. Form (2.4) is free from singularities and builds a hierarchy of leading and perturbing terms which might prove practical in future extensions or refinements.

2.2.1 *Nearly diurnal resonance*

The spectrum of the liquid core response has a resonance pole at the nearly diurnal frequency ω_{NDR}. It factors into the Love numbers as well as the coupling coefficients, i.e. the tilded symbols of (2.4), and is conveniently written

$$C_{\mathrm{NDR}}^{(\iota)}(\omega) = \frac{[\omega - \omega(O_1)]S_{\mathrm{bt}}^{(\iota)} + \Omega S_{\mathrm{ot}}^{(\iota)}}{\omega - \omega_{\mathrm{NDR}} - i\omega_{\mathrm{NDR}}/(2Q_{\mathrm{NDR}})}, \qquad \iota \in \{h, l\}. \tag{2.5}$$

Again, the off-resonance tide O_1 serves as a pivot. Here, Ω is the sidereal rotation rate, and S_{bt} denotes body tide resonance strength. S_{ot} is an oceanic interaction term; more details are given below. The results for an anelastic mantle (Wahr & Bergen 1986, equation 6.6) are accommodated in (2.5) after a few algebraic operations. Numerical values for (2.5) from the literature, transformed to comply with the factorisation scheme above, are given in Table A2.

The products of S_{ot} with $\bar{z}, \bar{l}^+$ and $\bar{w}^+$ are small with respect to all other terms, so that the placement of the oceanic part of C_{NDR} in front of the parenthesis in (2.4) does not cause accuracy problems.

The relations between the parameters of (2.5) and the dynamic properties of the core–mantle system are discussed in Wahr & de Vries (1989), Neuberg, Hinderer & Zürn (1987), Hinderer & Legros (1989), and Hinderer (1986).

The resonance frequency ω_{NDR} and its quality factor Q_{NDR} are preferably adopted from observations (Neuberg, Hinderer & Zürn 1987, gravity; Gwinn, Herring & Shapiro 1986 and Herring, Gwinn & Shapiro 1986a, b, VLBI). Currently available constraints on frequency shift due to the flattening of the Core Mantle Boundary (CMB) and the structure of the core near the CMB (Wahr & de Vries 1989) from theory or seismic tomography are rather weak. Anelasticity of the mantle and ocean tides appear unable to explain the observed frequency shift (Wahr & Bergen 1986). The inference of 5–6 per cent excess flattening of the core is based on the observations. The adoption of the gravity result for Q_{NDR} avoids a possible bias in the VLBI results due to the use of a tide module in the analysis software, the upgrade of which is the motive of the present study. The VLBI nutation result for ω_{NDR} is very close to the gravity result and is considered to be more accurate.

However, resonance strength results from tidal gravity are both weak and inappropriate for displacements. Probably Wahr & Bergen provide the currently best estimates. There is presently no tie between the anelasticity model advocated below and the viscoelastic parts of the NDR-strength parameters. They are—in contrast to perturbations in nutation—only weakly affected by excess core flattening and depend in the first case on mantle properties and tidal loading at the CMB. The results adopted in Table A2 from Wahr & Bergen refer to the upper limit of their rheological model; values between this and the elastic case are more likely, with reservation for yet unknown contributions from the inner core.

Ocean tides are capable to excite the core resonance by means of surface mass loading (Wahr & Sasao 1981). The effects pertain to westward rotating spherical harmonics of $(n, m) = (1, 1)$, the response being found in the (2, 1) load Love numbers resonant at ω_{NDR}. This co-oscillation is therefore accountable in the body tide model, and I attribute the term 'interaction' (of ocean loading tides with the NDR) to it. The relevant spherical harmonic modes of the ocean tide elevation are represented by the coefficients C_{21}^+ and ε_{21}^+ (notation according to e.g. Cazenave 1982). In response to a partial ocean tide k with a frequency ω_k the interaction strength parameters result according to

$$S_{\mathrm{ot}}^{(\iota)} = -i\frac{4\pi G\rho_w a}{5g\iota_2}\frac{\gamma(O_1)}{\gamma(\omega_k)}\bar{S}^{(\iota)}\frac{C_{21}^+(\omega_k)}{\Psi_k} \times \exp[i\varepsilon_{21}^+(\omega_k)], \qquad \iota \in \{h, l\}, \tag{2.6}$$

where $\bar{S}_{\mathrm{LL}}^{(\iota)}$ is the resonance strength of load Love number ι (Wahr & Sasao 1981) and $\gamma = 1 + k_{21} - h_{21}$ is the resonant ocean tide generating factor. Numerical values are given in Tables A2 and A3 (Appendix A), including solutions from the numerical tide models of Seiler (1989) and Schwiderski (1981a, b, c), combined with the North Atlantic model of Flather (1981) and adjusted for the resonant ocean tide effective potential in the case of Seiler's model. Although the interaction term is small, in fact less than the current accuracy of the body tide NDR-parameters, it is given here as a future option.

2.2.2 *Viscoelastic relaxation of the earth's mantle*

Thermally activated viscoelastic creep in the mantle causes additional, time-delayed deformation of the earth. Tidal forcing—sinusoidal in time—suggests the Fourier transform concept for the formulation of the response. Since the response is small and linear the Love number concept can be maintained by virtue of the correspondence principle,

now leading to frequency-dependent complex values. Qualitatively, amplitudes increase towards low frequencies, and phases lag with respect to the astronomical potential. Relaxation function $V_n^{(t)}(\omega)$ in (2.4) models this property; it is the transfer function of the viscoelastic, self-gravitating earth, speaking in terms of system theory.

In the following we concentrate on the case $n = 2$ since viscoelastic effects on the small tides at higher degrees appear negligible. Love number k_2 for the secondary potential perturbation is included in the analysis. It parametrizes also tidal variations of the earth's moments of inertia.

Since we are dealing with a causal system, the real and imaginary parts—alternatively the phase and the amplitude—of $V_n(\omega)$ are not independent. Instead, they constitute Hilbert transform pairs (*cf.* Dehant & Zschau 1989).

If a simple parametrization can be found for phase versus frequency, the Hilbert transformation to amplitude might be done analytically. To describe the complete spectrum only one additional amplitude coefficient is needed, conceptionally equivalent to the elastic (instantaneous) response. In application to (2.4) this constant has the task of 'calibration': the relaxation model is adjusted against a partial tide solution of an elliptic, viscoelastic earth. The case of a spherical earth is simpler: calibration would demand $V_n(\omega) \to 1$ as $\omega \to \infty$.

Relaxation spectra of body tide Love numbers have been presented by Wang (1986), based on a generalized Maxwell rheology of the earth's mantle capable to explain transient creep phenomena (anelasticity) over a wide range of frequencies (Zschau & Wang 1986). The same rheology was used by Dehant (1987) to extend the elastic model of Wahr (1981). Wang's results will be used in the following. Implausibly, Dehant's results show near-constant imaginary parts of the Love numbers below fortnightly periods.

Dehant's result for $\mathcal{I}m\, h_2$ at the fortnightly tide (M_f) agrees with Wang's data. This provides an opportunity to calibrate $V_2^{(h)}$ (*cf.* Appendix A, Section A2). Love number l_2, unspecified by Dehant, is seen to relax roughly three times more than h_2, giving a less strong calibration condition for $V_2^{(l)}$.

A Hilbert transform pair for attenuation α and phase ϕ,

$$V_2(\omega) = \exp\left[\alpha(\omega) + i\phi(\omega)\right]$$

will now be derived. In the present application the very long-period part is uninteresting. A log–log plot of Wang's Love numbers versus frequency (Fig. 1, crosses) suggests an empirical description of the phase spectrum

$$\phi(\omega) \cong \Phi_o \operatorname{sign}(\omega) \left|\frac{\omega_b}{\omega_o}\right|^p, \qquad 2\pi/18.6 \text{ rad yr}^{-1} < |\omega|, \tag{2.8a}$$

with only two parameters Φ_o and p for each Love number (*cf.* Table A4). For the present purpose the phase spectrum is artificially augmented by a linear characteristic

$$\phi(\omega) = \Phi_o \left|\frac{\omega_b}{\omega_o}\right|^{p-1} \frac{\omega}{\omega_o} = \Phi_1 \frac{\omega}{\omega_o}, \tag{2.8b}$$

$$|\omega| < \omega_b < 2\pi/18.6 \text{ rad yr}^{-1},$$

in order to preserve phase antisymmetry. The two branches

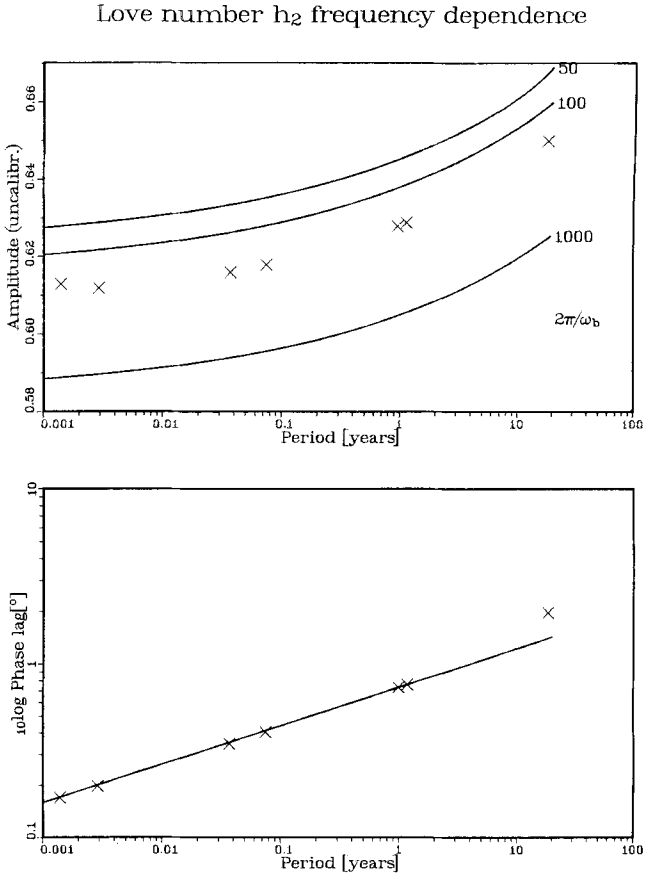

Figure 1. Comparison of the anelasticity model, equation (2.10), solid lines, with Wang's (1986) results, crosses. The attenuation spectrum is determined except for a constant, which has to be obtained from a calibration condition. The curvature of the model spectra depends slightly on the breakpoint frequency ω_b at which the two branches of the phase model join.

meet at the breakpoint frequency ω_b. This rather unrealistic phase law below ω_b has only limited impact in the frequency domain of concern.

The Hilbert transform from phase ϕ to attenuation α is

$$\alpha(\omega) = \alpha(0) - \frac{\omega^2}{\pi} \int_{-\infty}^{\infty} \frac{\phi(\sigma)\, d\sigma}{\sigma(\sigma^2 - \omega^2)}. \tag{2.9}$$

Substituting (2.8), (2.9) is evaluated at $\omega > \omega_b$ using the principal value theorem and power series expansion of the integrand with (2.8a). The resulting attenuation spectrum is

$$\alpha(p, \omega) = \alpha_o - \frac{\Phi_1}{\pi}\frac{\omega}{\omega_o} \log\left|\frac{\omega + \omega_b}{\omega - \omega_b}\right| - \frac{2\Phi_o}{\pi}\left(\frac{\omega}{\omega_o}\right)^p A(p) - \frac{2\Phi_1}{\pi}\frac{\omega_b}{\omega_o} \sum_{n=0}^{\infty} \frac{1}{2n + p}\left(\frac{\omega_b}{\omega}\right)^{2n} \quad \text{for } \omega \gg \omega_b. \tag{2.10}$$

Only a few sum terms are needed in the case of most tide frequencies. The constant $A(p)$ results from the limit $\varepsilon \to 0$ of the integral near the poles $\pm\omega$, $|\sigma \pm \omega| < \varepsilon$,

$$A(p) = \sum_{n=0}^{\infty} \frac{p - 1}{2n^2 + 2n + p - p^2/2} \tag{2.11}$$

and is given in Table A4.

The right diagram of Fig. 1 shows computed attenuation $\alpha(\omega)$ with ω_b as a parameter; the constant α_o is yet undetermined. The breakpoint frequency affects the curvature of the attenuation function only slightly. A satisfactory fit to Wang's data is obtained at $\omega_b = \pi/100\,\mathrm{rad\,yr^{-1}}$.

Calibration finally determines α_o, or—going from attenuation to amplitudes—the real constant v_{cal},

$$V_2^{(\iota)}(\omega) = v_{cal}^{(\iota)} \exp\left[\alpha^{(\iota)}(\omega) - \alpha^{(\iota)}(\omega_{cal}) + i\phi^{(\iota)}(\omega)\right]. \quad (2.12)$$

The relaxation spectrum yields a simple expression for the partial derivative with respect to phase parameter Φ_o,

$$\frac{\partial V_2^{(\iota)}}{\partial \Phi_o^{(\iota)}} = V_2^{(\iota)}(\omega) \frac{\alpha^{(\iota)}(\omega) - \alpha^{(\iota)}(\omega_{ref}) + i\Phi^{(\iota)}(\omega)}{\Phi_o^{(\iota)}}. \quad (2.13)$$

Time series of the displacement u and its partials with respect to Φ_o show sufficient dissimilarity (Fig. 2) to suggest $\Phi_o^{(h)}$ and $\Phi_o^{(l)}$ and the basic Love numbers H and L as the primary solve-for parameters in observation analysis. The assumption of an *a priori* fixed ratio of $\Phi_o^{(h)}/\Phi_o^{(l)}$, which would reduce the set to three parameters, is not advisable. It would oversimplify the different impact of stress relaxation on the two displacement components. The phase dispersion exponents $p^{(\iota)}$ are less suitable solve-for parameters unless very long-duration experiments are capable of discriminating long-period tides from aperiodic site offsets.

Provided that long-period UT variations are properly described through an effective Love number k_{eff},

$$d\Delta UT/dt = -\mathcal{R}e \frac{2}{3}\frac{k_{eff}}{C}(1+e)\frac{\Gamma_j}{a}\exp(i\omega_j t)$$

$$m_j = 0,$$

where $(1+e)$ denotes the correction term for secondary volume change (Yoder, Williams & Parke 1981, equation 24), C the dimensionless polar moment of inertia and

$$k_{eff} = k_2 - k_f(r_f/r_o)^5 + \text{oceanic contributions},$$

the relaxation function $V^{(k)}$ for k_2 and the tide harmonic expansion might be used in the earth rotation model. Wahr & Bergen (1986) approached the problem from perturbation theory applied to the rotational eigenmodes which are part of their normal mode equations. This is an alternative to the detour via Love number k_2. Their results, however, might suffer from uncertainties in the extrapolation of their rheological parameters from seismic to tidal periods. On the other hand, the present model underestimates the relaxation of the 18.6 yr tide, which is important for *UT* variations.

The parameters of the relaxation spectra, p and Φ_o, are empirical in that sense that they summarize observations of the behaviour of a model. So far they are formally unrelated to each other and call for an anchoring to rheological parameters such as an effective mantle quality factor Q, mean temperature or mean activation energy.

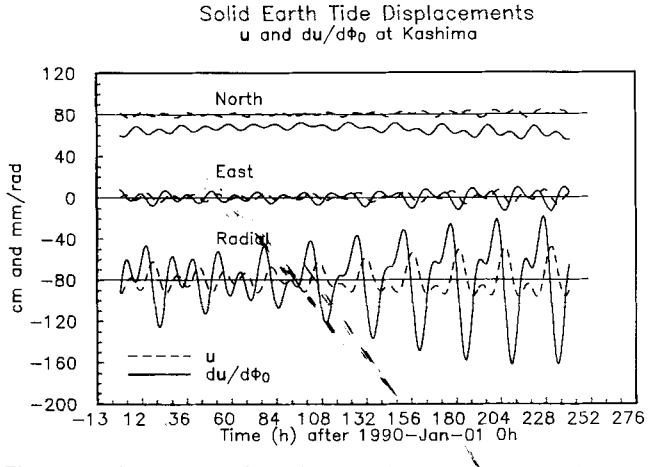

Figure 2. Time series of solid earth tide displacements (dashed curves) and their partial derivatives with respect to the phase lag parameter Φ_0 (solid curves). The quadrature phase relation between the two sets of time series favours the use of the phase lag parameter together with the wide band response amplitude as the first-priority parameters of the solid earth tide model to be resolved from observations. Enhanced importance of long-period tides for phase lag determination in the case of the north displacement partial is indicated by the offset of the signal.

2.3 Implementation into data analysis software

Computation starts with the compilation of the global arrays in (2.1), Ψ_j, χ_j, ω_j, n_j and m_j, from a harmonic tide development, χ_j evaluated e.g. at the central time of an experiment. Recent accuracy tests (Wenzel & Zürn 1990) favour the developments of Tamura (1987) and Xi (1987) which are based on refined ephemerides in the J2000 system. The developments are sufficiently stationary to be valid during the coming 20 years provided accuracy demands do not exceed one part in 10 000 of the total tide displacement. Care has to be taken to relate the conventional Legendre polynomials used here to the normalization used in the potential developments (*cf.* Appendix A, Section A1).

Predicted displacements, their rates and their partials are computed from the site-specific spectrum U and its partials using (2.3) and (2.4) into which (2.5), (2.12) and (2.13) are inserted. This requires storage of long arrays if the entire expansion of the tide spectrum is used. The limited duration of experiments motivates the search for a suitable truncation or condensation of the spectra.

Let each spectrum of the three displacement components be ordered by decreasing amplitude. Subscript 'c' denotes the component. Simply truncating the spectrum at line J_c, $|U_{cj}| < \varepsilon$ for $j > J_c$, causes an error e of the synthesized time series $u(J;t)$. Defining

$$e(\varepsilon) = \max_t \sum_c \{u_c^2[J_c(\varepsilon);t] - u_c^2(t)\}^{1/2}, \qquad 0 \le t \le 7500\,\mathrm{hr}$$

it turns out that more than 200 spectral terms are required for sites at almost all latitudes [*cf.* Table 2, based on the Büllesfeld (1985) expansion] to maintain millimetre accuracy.

In a second strategy a small set containing the frequencies of the J most significant tides forms a skeleton which reproduces the displacements of the total set of N terms at the central time of the experiment window. From there the spectrum is extrapolated forward and backward in time using only the skeleton frequencies:

$$\tilde{u}_c(t) = \mathcal{R}e \sum_{j=1}^{J} \tilde{U}_{cj} \exp(i\omega_j t), \quad (2.14)$$

Table 2. Sorted by decreasing amplitude, the first J tide constituents with amplitude greater than ε yield truncation error e of the synthesized tide displacements. Degree four tides are significant in the first column.

ε [mm]	0.01	0.03	0.1	0.3
N	550	400	230	140
e [mm]	0.09	0.28	0.9	2.5

where subscript 'c' numerates components as well as optionally computed parameter partials, and

$$\tilde{U}_{cj} = U_{cj} + \sum_{k \in \mathbb{S}_{cj}} U_{ck}. \tag{2.15}$$

The sets $\mathbb{S}_{cj}$ are defined by the nearest skeleton frequency:

$$\mathbb{S}_{cj} = \{J < k \leq N \mid |U_{ck}| > 0 \wedge |\omega_k - \omega_j| \leq |\omega_k - \omega_l| \; \forall l \leq J\},$$
$$j = 1, \ldots, J. \tag{2.16}$$

Zero tides (e.g. long-period east displacements) are thereby rejected. The number J depends on the duration of the experiment and an accuracy threshold ε_c, demanding that

$$\left| \mathcal{R}e \sum_{j=1}^{J} \sum_{k \in \mathbb{S}_c} U_{ck} [\exp(i\omega_j T) - \exp(i\omega_k T)] \right| < \varepsilon_c \left(\sum_{j=1}^{N} |U_{cj}|^2 \right)^{1/2} \tag{2.17}$$

at the end of the time window T. if the parameter partials were derived from the condensed spectra instead, important information, e.g. the frequency characteristic of the nearly diurnal resonance, might become lost.

As an example for (2.17) the *a prosteriori* error

$$e_c(t) = \max_{\tau < t} |\bar{u}_c(\tau) - u_c(\tau)|$$

is evaluated for a site at 30° latitude (*cf.* Fig. 3) to determine a relation between J and ε_c. It turns out that $J \cong 50$ skeleton constituents achieve an internal accuracy of 0.2 mm during a 36 hr experiment. The values of ε_c for each component are given in the legend of Fig. 3. A skeleton is to be stored for every site, component, and parameter partial, together with pointer arrays, i.e. the sets $\mathbb{S}_{cj}$.

The scheme above retains the essential information in much shorter data arrays. Automated determination of J for each individual component and parameter partial accomplishes this task at the expense of computational effort at the preprocessing stage, but spent only once for each participating site. Since the sensitivity of VLBI to displacement velocities (appearing in the adjustment equations for delay rate) is limited, the associated expressions are preferably computed from the condensed spectra.

A development version of a tide subroutine package for the pre-processing stage (computation of thereoreticals) has been constructed such that model parameters can be flexibly redefined; spectra of parameter partials are then easily obtained by divided differences.

2.4 Discussion: achieved improvements

The demands listed at the beginning of the previous chapter could be widely fulfilled. Studies are suggested to provide

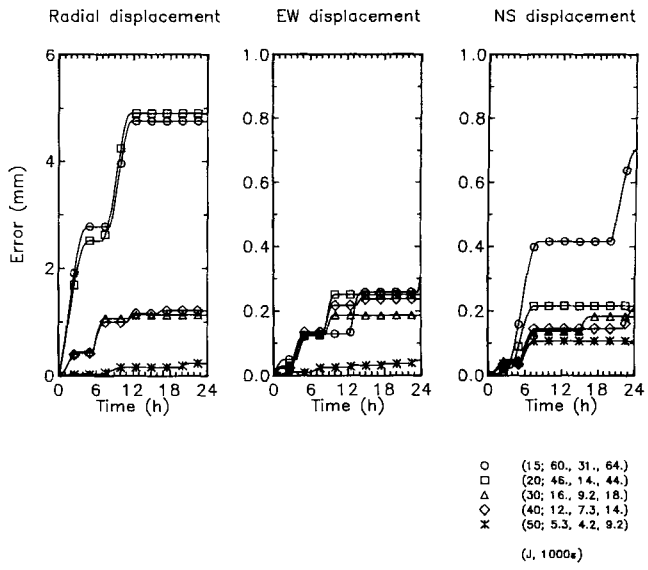

Figure 3. A skeleton spectrum comprising only the frequencies of the J most important tides (equations 2.14, 2.15) allows Fourier extrapolation of tide displacements within a certain time window from a given central epoch with an internal accuracy e (displayed against the ordinate). The *a priori* error threshold ε (equation 2.17) and the associated skeleton length J are indicated in the legend. $J = 50$ suffices to achieve an accuracy of 0.2 mm during a 36 hr experiment. The example shown is for a site at 30° latitude centred on the spring tide period of 1990 April 25 0:0.

more stringent physical ties of some of the model parameters to actual physical parameters, mainly for the part of rheology. The relation of the spherical harmonic order coefficients β_{2m} to the flattening parameter might also need further substantiation.

Comparing with the currently used method as described in IERS-Standards (McCarthy 1989) and applied in various software packages, the following improvements are noted ('OM' and 'NM' denote the 'old' and the 'new' model, respectively).

OM is based on planetary ephemeris data—time series of distance vectors for moon and sun with respect to the earth. They have to be acquired for each observation campaign. OM avoids formulations in the frequency domain.

The use of harmonic development of the tide potential makes NM independent of this supply, and—more important—has provided the basis for frequency domain formulations, which are essential in the case of the NDR and viscoelastic relaxation.

Here, OM had to apply shortcuts in order to achieve its 5 mm accuracy. For instance, a single correction term for the tide K_1 was introduced to account for the NDR. The CALC/SOLV package for VLBI uses a 'lag angle of the tidal bulge', a small rigid rotation of the displacement field around the ecliptic pole. The same lag angle is applied to both radial and tangential displacements.

NM formulates explicitly the perturbations due to earth ellipticity. OM achieved some degree of compensation for these effects by computing the external tide potential at the geocentric distance of the site and dividing by ellipsoidal gravity in order to obtain units of displacement.

As regards implementation into data analysis software, NM is more voluminous. However, storage requirements and computational effort can be reduced according to suggestions in Section 2.3.

2.5 Discussion: application

Four key parameters for the observation equations are suggested: H, L, $\Phi_o^{(h)}$ and $\Phi_o^{(l)}$. The dependence on almost all parameters in equation (2.4) is linear, so that parameter partials are most easily obtained by lowest order divided differences. Although this costs twice the computation effort, it pays back in terms of flexibility and formula coding.

Access to the NDR parameters—frequency, quality and strength is provided. Resonance frequency and quality enter non-linearly. However, iterative adjustment methods are unrealistic to suggest; qualified initial values exist.

A set of parameters of the proposed model may be determined from carefully selected observation campaigns. Presently, the observation schedule and data analysis routines of the regularly repeated but disjointedly analysed VLBI campaigns IRIS or POLARIS (Herring *et al.* 1983; Carter *et al.* 1985; Schuh 1989) are not ideal from the tidal point of view.

The capability to resolve model parameters and to discriminate perturbations depends greatly on source and site geometry (Schuh 1987; Dermanis & Grafarend 1981). An example is ocean tide perturbations of pole position and UT1 from IRIS experiments (Brosche *et al.* 1989) where contamination from the nutation model was a problem. The limited time coverage of observations or disjoint analysis of repeated experiments cause a reduction of resolving power when dealing with periodic processes. In the case of earth tides one clearly needs both spatial and frequency coverage. Particularly, long north–south baselines must be included.

In the regular campaigns, however, gain is expected in terms of validity, consistency, and accuracy of the new tide module, even if its parameters are kept fixed.

The tide model presented so far is still incomplete. Effects which are inseparable from the body tides have not been discussed yet.

The presence of ocean loading perturbations—which show a high degree of variability with respect to frequency and position—has traditionally favoured the use of narrow-band observation models for the analysis of long duration tide recordings (e.g. Schüller 1976, 1986). These estimate the sum admittance of the body tide and cotidal perturbations. This sum may randomly vary on small frequency scales. Predicted perturbations are subtracted after the fit (operation in the frequency domain). Constraints that would utilize the spectrally smooth behaviour of the Love numbers are usually not applied.

The model presented here dwells on the wide-band systematic character of the solid earth response. Predicted ocean tide loading effects and other perturbations (e.g. climatic effects) are to be subtracted from the primary observables as a part of the site-specific information. Since this is a time domain operation, one is not restricted to purely harmonic cotidal signals. The harmonic part, however, computes conveniently on the basis of the lunisolar tide spectrum.

Although also earth orientation perturbations at tidal frequencies can be described on a subset of the harmonic development above, the response of the earth depends on sufficiently many other parameters (low harmonic degree ocean tide response coefficients, decoupling of the core in rotational modes, effective Love number k_2) that the parameter overlap with the model above is rather small. The following VLBI analysis session is therefore still hypothetical.

(i) Observations from 5 day experiments, involving sites on all tectonic plates, covering one to several years.

(ii) Parametrizing ocean tide effects on ΔUT and the orientation angles with respect to frequency. Parametrizing the effect of core decoupling on the rotational response with respect to frequency.

(iii) Applying the corrections for ocean loading tides.

(iv) Solving with emphasis on the consistency of the viscoelasticity parameters and the frequency offset of the Chandlerian motion (Zschau 1986). Also test the consistency between the departure of long-period ocean tides from equilibrium and the lengthening of the wobble period.

(v) Solving simultaneously for the frequency of the NDR of the core from tides and nutations.

Recently developed analysis methods applying Kalman filtering techniques (Herring, Davis & Shapiro 1990) bear the power to extend the effective observation duration of VLBI experiments if applied to all model parameters. This provides the prerequisite for the resolution of long-period phenomena, among others the low-frequency tides.

3 OCEAN LOADING EFFECTS

The amplitude and phase relations of ocean loading effects versus the solid earth tides are strongly site and frequency dependent. A parametric model would have to consist of a spherical harmonic development of hydrodynamic eigenmodes, augmented with corrections for non-linearities in the ocean response. Such an approach is not feasible, partly because of the tremendous amount of parameters involved and partly because of convergence problems (Groten & Brennecke 1973).

Probably the best choice is instead to treat ocean loading effects as a site specific perturbation. The phase angles of these displacements show systematic alignment with the body tides (Scherneck 1987). Ignoring the perturbation can introduce a bias in the estimated body tide parameters. A bias of the body tide parameters, however, might still occur if ocean loading errors are not randomly distributed with respect to geographic location or frequency.

Ocean loading effects are mediated by the response of the earth to surface stress and mass potential. The Green's function of the point load involves an infinite sequence of load Love numbers for all SH degrees (Farrell 1972). The displacements induced by the point load are

$$du_r = \mathscr{G}^{(h)}(\vartheta)\, dm = \zeta \frac{G\rho_w a}{g} \sin\vartheta\, d\vartheta\, d\lambda \sum_{n=0}^{\infty} h'_n P_n(\cos\vartheta) \tag{3.1a}$$

in the radial component, and

$$du_{\alpha} = \mathcal{G}^{(l)}(\vartheta)\, dm$$

$$= \zeta \frac{G\rho_w a}{g} \sin\vartheta\, d\vartheta\, d\lambda \sum_{n=0}^{\infty} l'_n\, \partial_{\vartheta} P_n(\cos\vartheta) \qquad (3.1b)$$

in the horizontal component along the direction α from the load to the field point. The arc distance between the load and the field point is denoted by ϑ. The projection of the unit vector $\mathbf{e}_{\alpha}$ on the local north and east directions yields the horizontal displacement components at the observing site

$$du_N = -\cos\alpha'\, du_{\alpha}, \qquad du_E = -\sin\alpha'\, du_{\alpha}, \qquad (3.1c)$$

where α' is the azimuth of the load at the site, counted clockwise from north.

The Green's functions $\mathcal{G}(\vartheta)$ are evaluated on a set of distance angles and stored in tables. They are interpolated to actual distances at the stage of intergration of (3.1). The tide elevation ζ is taken from global tide maps which represent amplitudes Z and phases δ for specific partial tides j

$$\zeta = \zeta(j, \varphi, \lambda, t) = Z_j(\varphi, \lambda) \cos[\omega_j t + \chi_i - \delta_j(\varphi, \lambda)]$$
$$= \mathcal{R}e\, Z_j(\varphi, \lambda) \exp i(\omega_j t + x_j). \qquad (3.2)$$

The tide charts of Schwiderski (1980a, b, c) have found wide acceptance. Methods to approximate the integral of (3.1) are reviewed in Baker (1985). Neglecting small-scale features like improved coastline resolution or lateral heterogeneities of crust and mantle, loading results can be produced in the form of global maps (Francis & Mazzega 1990). Additional discussion follows below.

3.1. Loading Green's functions

3.1.1 Point load approach and lateral heterogeneities

The point load character of the loading problem and its Green's function solution suggests that relatively small-scale lateral heterogeneities of earth structure are able to perturb spherical symmetry. These effects are expected to be more important than in the body tide case, where ellipticity—the dominant lateral heterogeneity of the earth—produces perturbations of degree two Love numbers of the order of the flattening parameter, and where the generating potential is confined to low SH degrees. In particular, the Green's functions have a singularity at the origin with ϑ^{-1} as an asymptote. Near the point load the deformation field is predominantly local, a consequence of the principle of Saint-Venant.

Farrell (1972) computed Green's functions for continental and oceanic structure; he found that a change of structural parameters down to a depth of 200 km affected the Green's function within a spherical cap of approximately 200 km radius. This one-to-one depth–distance relation was systematically studied by Rabbel (1982), confirming its validity for thin, anomalous layers from the surface down to about 400 km. Hence, the loading effects at the coast of a 200 km wide continental shelf are sensitive to the continental structure. For increasingly narrower shelves, the response character changes successively to the oceanic crust type.

The classical results of Farrell have been refined in recent

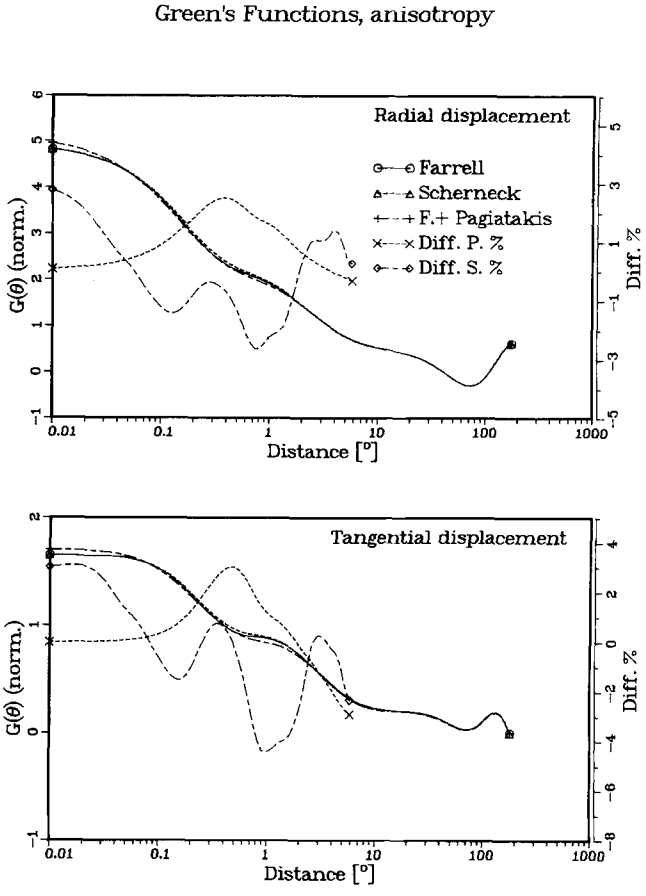

Figure 4. The loading Green's functions of Farrell (1972), Scherneck (1990) and Pagiatakis (1990), the latter of which includes effects from anisotropy of mantle material. Also shown are their percentage differences with respect to Farrell's functions. The radial Green's functions (top diagram) as well as the tangential ones (bottom) are normalized with respect to the level-surface perturbation due to the gravitational attraction of a unit point mass.

studies on the tidal loading problem, incorporating more realistic constitutive laws for the reheology of the earth. Wang (1986) has computed loading Green's functions using the rheological model of Zschau (Zschau & Wang 1986). The most prominent property is a frequency-dependent increase of the deformation in a distance interval between 0.3° and 3° as an effect of anelastic relaxation in the asthenosphere; at the Chandler Wobble frequency, $\mathcal{G}^{(l)}$ is about 50 per cent larger than in the case of short-period tides.

Recently, Pagiatakis (1990) added effects from earth rotation, Maxwell rheology, and anisotropy of the elastic moduli as specified by the PREM earth model of Dziewonski & Anderson (1981). As regards the effects of earth rotation mediated by the Coriolis virtual force, the work is not convincing: the displacement field was only analysed for its spheroidal part (*cf.* Aki & Richards 1980, chapter 8). The neglect of the toroidal part leads to the implausible result that the loading Green's functions maintain their spherical symmetry. The model further mixes parameters for a (steady state) Maxwell rheology based on results from studies on very slow deformations—the fastest being post-glacial rebound—with those of a (transient)

anelastic rheology. In particular, the dash-pot elements of the corresponding model bodies (Maxwell and Kelvin–Voigt) are given identical roles, which appears doubtful. Zschau (1986) concluded that steady state rehology cannot provide an explanation for dissipation in the frequency domain between seismic waves and Chandlerian motion. A broad absorption band model, using e.g. a distribution of strain retardation times by means of chaining Kelvin–Voigt bodies appears more realistic.

Most interesting are the results of Pagiatakis as regards anisotropy. Since anisotropy between vertical and horizontal seismic wave velocities is compatible with decoupling of transverse horizontal shear from normal surface stress, the displacement field can be fully represented by spheroidal components. Pagiatakis obtains relative changes of load Love numbers of less than 2.5 per cent for l'_n and 1.9 per cent for h'_n. A comparison of the associated Green's functions with Farrell's (using Pagiatakis 1990, fig. 1) is shown in Fig. 4. The maximum anisotropy effect occurs as expected at the 'asthenospheric distance' of 2°.

In order to compare the effect from loads within zonal rings at different distances, the order of magnitude of radial displacement can be estimated from

$$\mathcal{G}^{(h)}(\vartheta)\, dm = \zeta C g^{(h)}(\vartheta) \frac{\sin\vartheta\, d\vartheta\, d\lambda}{2\sin\vartheta/2},$$

the mean value—denoted by $\langle\cdot\rangle$—of which is

$$\langle|u_r|\rangle \cong 4\pi CE[\sin\vartheta/2]_{\theta_1}^{\theta_2} g^{(h)}(\theta_m)\langle|\zeta|\rangle. \qquad (3.3)$$

Here, C contains the physical constants; E denotes an effective tide coverage and consists of two factors, A and I, for the azimuthal extent of the zone and the interference of tide phases within the zone respectively. Distance θ_m is the effective distance of the ring area, $\theta_1 < \theta_m < \theta_2$. Equation (3.3) is used for the evaluation of some of the error estimates of Table 4.

Straining (3.3) to the global case for an inland station that typically experiences 1 cm or radial displacement from 0.5 m global ocean tides, one obtains a plausible value for the product gI of 0.05. The interference factor approaches unity as the outer radius of the zone shrinks to zero; g approaches roughly a value of six on continental crust or four on oceanic crust respectively.

3.1.2 *Disc loads and integrated Green's functions*

Approximation of (3.1) by summation over a gridded ocean model is referred to as the point load convolution method. The point load position is the centre-of-mass of the finite surface element (Jentzsch 1985).

Distributed loads instead of point masses are more suitable for the discrete convolution method. A circular disc attenuates the short-wavelength response and its effect can be accounted for inside the inflinite sums of the Green's functions (3.1a and b), speeding up convergence. Kummer's transformation provides a second method to facilitate the computation of these sums.

Francis & Dehant (1987) have pointed out problems with the use of Kummer transforms for the point load case—for which *analytical* expressions exist—while the remaining explicit summation treats the disc load case. However, valid Kummer transforms for the disc case can be obtained from *numerical* integration of the point load Kummer transform over the disc. The resulting improvement is not more than one per thousand (Scherneck 1990).

As an alternative to a circular disc Goad (1980) integrated the loading Green's function over surface ring sectors. These sectors form a template centred on the observing site. The P_n's in (3.1) are replaced by their integrals over a template element, in which the tide heights are assumed to be piecewise constant. Goad developed his method mainly in application to gravity.

The advantage of faster convergence of the Integrated Green's Function (IGF) is counterbalanced by the need to project the global ocean grid onto the template. In the case of the displacement components, point loads or circular discs present no serious convergence problems.

The effect of the topographic height of the observing site upon the Newtonian attraction term, which appears in the gravity and tilt components, can be computed in closed form using the IGF. Goad extended this concept to the deformational terms as well. As a result, a factor of $[a/(a+h)]^n$ multiplies the response to forcing at a particular degree n. It appears doubtful whether this would hold in the case of sharply confined topographic features.

3.1.3 *Transverse stress response*

Transverse surface stresses result at bathymetric slopes under tidal loads. Merriam (1986) has devised a Green's function approach for transverse stress boundary conditions. The displacement effect is expected to be largest at coasts near a steep continental slope, e.g. in the case of sites in eastern Japan.

The three-component displacements u due to a horizontal force acting upon a surface element ds are given by

$$df = \nabla b g \rho_w \zeta\, ds, \qquad du = \mathcal{J}(\vartheta, \alpha)\, df,$$

Table 3. Site displacements in the radial, north–south and east–west directions due to tangential stress induced by ocean tide loading on topographic slopes. Site location is given in degrees longitude and latitude. The Green's functions of Merriam (1986) have been used.

Site lon. lat.	Tide	Displacement amplitude [mm] and phase Radial		North-South		East-West	
Onsala	M_2	$5\cdot10^{-8}$		0.14	-89°	0.14	158°
11.9, 57.3	K_1	0.01	-29°	0.03	174°	0.03	86°
Vandenberg	M_2	0.03	-14°	0.22	-30°	0.48	167°
-120.6, 34.6	K_1	0.03	54°	0.16	25°	0.35	-149°
Kashima	M_2	0.05	31°	0.14	44°	0.30	25°
140.7, 36.0	K_1	0.04	-149°	0.11	-137°	0.19	-140°

where f is the horizontal loading force, b is bathymetry, and $\mathcal{J}$ is a 3×2 matrix of transverse stress Green's functions (MTGF) multiplied with projection matrices of the force and displacement field at load and field points respectively on the azimuth α.

A continental slope $|\nabla b|$ is rarely greater than 0.1, and the MTGF in the near field behaves asymptotically similar to the normal stress Green's functions; both have similar amplitudes. Thus, one can expect at least one order of magnitude smaller effects from transverse loading. The limited area covered with slopes and their unsystematic orientations on the global scale attenuate net displacement effects further. Computed effects amount to one tenth of a millimetre or less (*cf.* Table 3).

3.2 Ocean tide models

The accuracy of ocean tide models is crucial for the computation of loading effects. The problems encountered in this context can be classified into (a) model errors on the global scale; (b) model errors near the observing site; (c) mass conservation. Distinction between the first two items refers to the importance of tides near an observing site: roughly one half of the loading effect results from tides within a distance of 2000 km. Model errors within this zone might be highly correlated. Remote zones, on the other hand, contribute with approximately equal weight, allowing assessment of random errors on the global scale.

Assuming stationarity, global random errors can be characterized by variance and correlation of errors between neighbouring points:

$$\sigma_\zeta = \mathrm{var}\,(\Delta z_j)$$
$$\mathrm{cov}\,[\Delta z_j(r_1), \Delta z_j(r_2)] = f(\sphericalangle r_2, r_1)\sigma_\zeta. \qquad (3.4a)$$

Schwiderski estimates his model to be accurate at the 5 cm level, i.e. $3\sigma_\zeta = 0.05$ m with some optimism. Previous studies (Hsu 1987; Woodworth 1985) did not consider correlation of errors and therefore tend to underestimate error propagation into the loading effects. Preliminary results (Scherneck 1989) indicate an increase by a factor of four to five of the loading effect error with respect to the uncorrelated case, assuming a correlation model

$$f(\vartheta) = \exp(-\alpha\vartheta). \qquad (3.4b)$$

A value of $f(1°) = 0.4$ was found in a comparison of the Schwiderski and Flather (1981) models of the North Atlantic.

Mass conservation is violated if tide mass cyclically disappears and reappears in the model. Schwiderki's models are driven by tide gauge data, i.e. the hydrodynamical solution of ζ is replaced by observed tides at mareographic sites. This interpolation scheme cannot easily conserve mass since many tide gauges are mounted at the coast where tide mass and tide elevation are related via the water-covered fraction of a grid element. Regardless whether the 1° resolution of the ocean model grid or high resolution of coasts obtained from a 5′ topography file is used, the mass budget

$$\Delta m_j = \sum_k \rho_w z_j(\varphi_k, \lambda_k)\,\Delta s_k \neq 0 \qquad (3.5a)$$

turns out to be significant for the loading effects at the 10 per cent level. In (3.5a), k numerates the model grid, and Δs is the water-covered area of a grid element. Mass conservation can be forced *a posteriori*, and its loading effect can be estimated to first order (Agnew 1983). The procedure of subtracting a homogeneous co-oscillating ocean layer for obtaining a mass conserving model $\hat{z}$,

$$\bar{z}_j(\varphi_k, \lambda_k) = z_j(\varphi_k, \lambda_k) - \Delta m_j \left(\rho_w \sum_k \Delta s_k\right)^{-1} \qquad (3.5b)$$

has proven successful in application to tidal gravity (Ducarme, personal communication). An uncertainty of 20 to 50 per cent of the correction might have to be accepted, however.

The dominating impact of loading tides in the vicinity of an observing site requires ocean tide models to be accurate on the regional scale. In the region close to an observing site, the following improvement is suggested. Since Schwiderski's models are driven by tide elevation data, and ocean loading is an effect of tide mass, refined coastlines can be used to compute the effective loading mass of coastal grid cells. Where on the one hand a tide gauge has pinned the model, the actual tide mass is reduced according to the land–ocean distribution within that grid cell. Those grid cells where the solution fulfils the continuity equation on the other hand conserve mass, and this mass can be redistributed over the corresponding high-resolution grid cells.

Specific regional tide models are suggested for ocean areas not or inaccurately represented in the global set (Scherneck 1990a). A general estimate of their impact on the computed loading effects cannot be given; in extreme cases they might exceed 1 cm after all tide constituents have been collected. Regional models are particularly needed for sites on Mediterranean islands and peninsulas, around the Irish sea, and near the Sea of Japan. These regions are blanked out in Schwiderski's models.

Combining a regional model with the global model changes the total mass balance. Mass flow discontinuities occur at the boundary between the models. The mass budget of a regional model with open, driving boundaries, impermeable coastlines, and negligible numerical mass loss depends on the currents at the open boundary. The decision as to whether the regional model improves the global mass budget (i.e. whether the co-oscillating layer also should cover the regional model's area) has to be based on the reality of the currents prescribed along the open boundaries.

Estimates of the uncertainty of the computed loading effects due to the uncertainties of the ocean tide and solid earth models are given in Table 4. Only the radial component is shown; tangential displacements are usually of the order of one third. Ocean tide models cover only a limited set of tide constituents. This truncation problem requires careful consideration. It is in principle related to the convergence problem of the harmonic development of the astronomical tide. Tide spectra can be understood as a product of modulation of a finite set of frequencies, where mixing occurs along a non-linear system characteristic. The cascase of intermodulation products forms a countably infinite set of background frequencies, on which the set of principal, declinational, and first-order elliptical tide waves stand out as a foreground line spectrum. The background

Table 4. Catalogue of error sources in ocean loading computations.

Error of the computed loading effects ...	Δu, σ_u [mm]
(A) ... due to loading Green's function (Eq.3.3)	
$0.01 \leq \vartheta \leq 2°$ (oceanic vs. continental crust, site near coast)	
$A = 0.5$, $I = 1$, $\varrho = 4$, $\Delta\varrho = 50$ %, $\zeta = 1$ m	10
Relative uncertainty $\Delta\Delta\varrho = 10$ %	2
$0.3 \leq \vartheta \leq 3°$ (asthenosphere; anelastic relaxation short period tides; anisotropy)	
$A = 0.6$, $I = 0.8$, $\varrho = 3$, $\Delta\varrho \leq 10$ %, $\zeta = 0.5$ m	≤ 1
(A.a) ... due to neglect of transverse stress	≤ 0.5
(B) ... due to ocean model, ...	
(B.a) ... global, random errors (Eq.3.4)	
$\sigma_z = 50$ mm, $\alpha = 0.4$	
σ_u Europe, near coast	0.5
" inland	≤ 0.3
North America, east coast	0.7
" " , west coast	0.6
(B.b) ... failure of mass conservation	
M_2 tide (Schwiderski)	
site on continent, near coast	0.3
inland ($\geq$ 300 km from coast)	≤ 0.15
on Pacific island	0.6
K_1 and O_1 tides, site on Pacific island	≤ 0.1

contributes at least one tenth of the tide signal. In the ocean tide case the problem is enlarged due to additional non-linearity of the ocean response and due to meteorological forcing. Improved ocean tide models require therefore the simultaneous presence of a number of major tides in addition to the solved-for wave. As a consequence of the irrational spacing of the basic (astronomical) frequencies the solution becomes explicitly time dependent.

The following illustrative example is given. There are two small companions to the tide M_2, separated by plus and minus one cycle per year (Darwin symbols α_2 and β_2). In addition to the linear response to these three tides, the ocean tide is modulated due to non-linearity. Annual variations of the water level are seen to perturb the M_2 especially on shallow shelves (Baker & Alcock 1983). This gives rise to spectral power at α_2 and β_2 being much greater than the linear response to these small tides. Power in the interval enclosing α_2, M_2 and β_2 results from the fact that the long-period sea level variation is not purely sinusoidal. Hence, extrapolation or interpolation of loading tide using linear dependence on the amplitudes and phases of the astronomical tide alone cannot account for the modulation effect.

A preliminary estimate of the loading effect due to the neglected ocean tides is 5 mm for sites up to 200 km inland. A similar figure was obtained in Scherneck (1983), where only linear interpolation and extrapolation were considered. Since non-linearity is effective in shallow waters only, an admittance of 0.001 to 0.005 for radial displacement versus height of the non-linear tide might serve as a rule-of-thumb.

A lower bound is obtained by linear superposition of the unmodelled tides, using interpolation and extrapolation of the tide spectrum (*cf.* Section 3.3). Fig. 5 illustrates the situation for the Kashima site, which is situated near the Pacific coast of Japan. There, displacements amount to 4 cm due to the 11 modelled constituents whereas the interpolated constituents contribute roughly 5 mm. Non-linear ocean tide interaction would increase this figure.

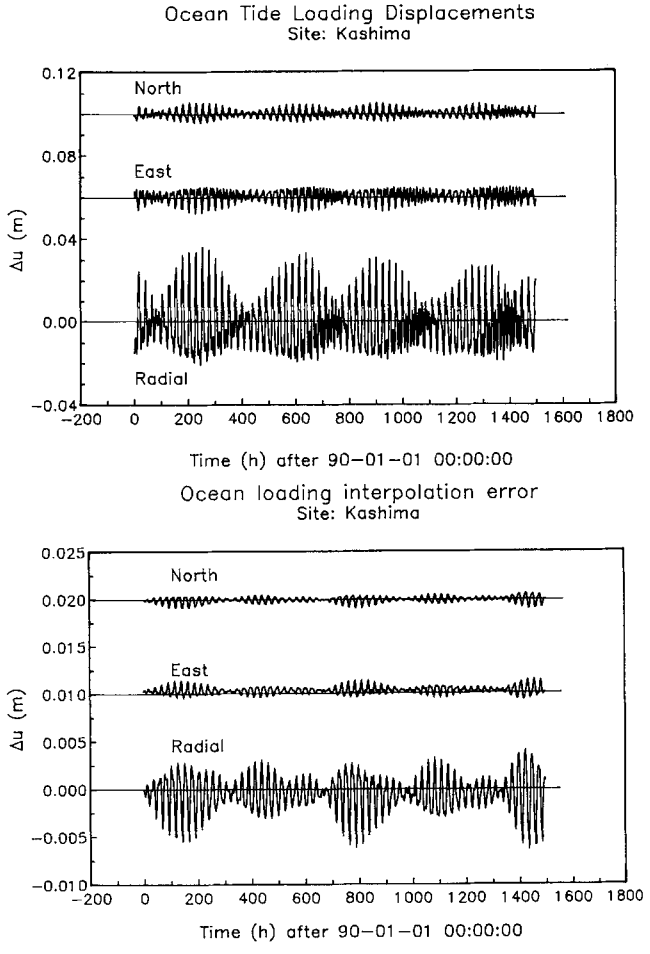

Figure 5. Ocean tide loading displacements for the Kashima site. Top diagram: computed from the 11 constituents of Schwiderski's models and 462 constituents supplemented by spectral interpolation, using the tide potential development of Büllesfeld (1985). Bottom: the contribution due to interpolation (equations 3.8, 3.9) of the load spectrum.

3.3. Providing ocean loading coefficients

Fully time-dependent modelling of tides can solve the non-linear tide problem (Malone & Kuo 1981; Kuo, Chu & Chen 1986); however, ocean loading parameters for distinct tide waves are then no longer applicable. Instead, station displacements would have to be communicated in the form of time series for each particular experimental campaign. The costs and work intensity of this kind of procedure are not very favourable. On the other hand, a fully time-dependent ocean tide model could simultaneously include the response to air pressure and wind stress. The total atmosphere and ocean loading problem could then be solved in one stroke, modelling displacements of maximum 50 mm (Van Dam & Wahr 1987) at probably 1 mm accuracy or even better.

Appendix B specifies ocean loading coefficients A_j in the traditional form, i.e. amplitudes and phases for the major partial tides independent of time. Results for many more stations are available from the author. They are the result of the point-load approximation to

$$A_{jk}(\phi, A) = \int \bar{z}_k(\varphi', \lambda') P(\alpha') G(\vartheta') \rho_w \, d\sigma' \tag{3.6}$$

with above-mentioned refinements, k numerating the 11 partial tides of Schwiderski's model, $G = [\mathscr{G}^{(h)}, \mathscr{G}^{(l)}, \mathscr{G}^{(l)}]^T$, $P = \text{diag}\,(1, \sin, \cos)$. The displacements (3.6) and Table B1 are in a (vertical, west, south)-oriented system. The total tide displacement is then

$$U_j = U_j^{(bt)} + \exp(i\chi_j) \begin{pmatrix} 1 & 0 & 0 \\ 0 & 0 & 1 \\ 0 & -1 & 0 \end{pmatrix} A_j^* \tag{3.7}$$

in the $(\mathbf{r}, \vartheta, \lambda)$ system. The astronomical argument χ_j in (2.1) is compatible with Schwiderski's phase definition†. Complex conjugation (asterisk) of the loading coefficients is due to oceanographic phase convention.

Preliminarily, the following linear scheme is used in order to obtain at least a first account of unmodelled tides:

$$\Delta U_j = A_k \frac{\Psi_j}{\Psi_k}, \qquad J_b(k) \le j \le J_e(k), \qquad n_j = 2, \tag{3.8}$$

where k refers to the modelled ocean tide constituents and the J's specify the begin and end (subscripts 'b' and 'e') of the associated tide band. A natural band structure is defined by the increments of the integer argument numbers $q_{\tau j}$ ($\equiv m_j$) and q_{sj} pertaining to the astronomical arguments τ and s (mean lunar time and mean tropical lunar longitude) of tide j: the fundamental bands due to m_j (long-period, diurnal etc.) are structured into sub-bands due to q_{sj}. The limits of these sub-bands are indicated by J_b and J_e in (3.8). Some sub-bands will be lost, however, if no ocean tide model representative for that band exists (e.g. L_2; the species below N_2 and above K_2).

† The comment in the IERS-Standards document on this phase problem is ambiguous. There is no phase disagreement of $\pm\pi/2$ in the case of the diurnal waves if equation (13) in Cartwright & Tayler (1971, pp. 52–53) is properly applied. They use cosines and sines if $n + m$ is even or odd respectively, whereas Schwiderski (and most harmonic tide developments) uses a cosine argument shift of $\pi/2$ if $n + m$ is odd.

The loading effect of bands dropped because of q_s might be interpolated,

$$A_j = \Psi_j \left(B_k + \frac{B_{k+1} - B_k}{\omega_{k+1} - \omega_k} (\omega_j - \omega_k) \right),$$
$$m_{k+2} = m_k = m_j, \qquad n_{k+1} = n_k = n_j = 2,$$
$$B_k = A_k / \Psi_k, \tag{3.9}$$

and even be extrapolated to the corners of the principal bands. Loading effects from (not modelled) degree three tides are thereby excluded. It might be suggested to compute the error of the above approximations from world-wide observations of tide heights, for each location solving for the (11) modelled constituents by least-squares, filling in the interpolated constituents, investigating the residual spectrum with emphasis on coherence relations between tide gauge sites, and from this estimating the loading effects.

5 CONCLUSIONS

The earth tide model presented is feasible to be incorporated into data analysis procedures in VLBI and laser ranging. It contains four basic parameters which can be adjusted from observations, and additional resolvable parameters can easily be obtained if desired. Emphasis was given to relate the model parameters to quantities which are typically given in solutions of the problem of (in-)elastic deformation of an ocean-covered, self-gravitating, rotating planet with a liquid core. Recent results were quoted from the literature.

The model is principally capable to supply displacement information with millimetre accuracy. Attention was given to maintain physical consistency with respect to the causality condition and the geometry of the problem. The crucially limiting factor on accuracy is ocean loading, where in extreme cases—sites on complicated crustal structures and situated near coasts with large amplitude tides—the accuracy aim might not be fulfilled.

A harmonic tide development forms the basis of the (frequency domain) response model. In application to VLBI and laser ranging, the same tide potential can be used for the earth rotation and polar motion perturbation model. It is suggested to revise the presently used software, to identify the group of processes to be modelled which relate to the tide potential and to restructure the code accordingly. Fourier interpolation using a skeleton spectrum with roughly 50 constituents per component and parameter-partial suffices to compute tides for a typical 36 hr experiment, maintaining submillimetre internal accuracy.

About 20 global parameters, of which four are the major candidates for estimation, control the solid earth tide model; 33 coefficients per site are required for the ocean loading part, which at this stage offer only limited access for adjustment from observations. Further studies are required to strengthen the ties between suggested rheological parameters in the observation equations and models of the anelastic behaviour of the earth's mantle.

Perturbations not taken up above concern atmospheric, solar radiation tides; their effect is accompanied by perturbations of the radio wave or light path through the atmosphere, and by much greater thermal effects on the receivers.

Refinement of the parameters used in the model can be expected from continued studies of tidal gravity, but also using the space techniques of VLBI and laser ranging.

The model covers only the stationary displacements related to tides and loading. Non-stationary perturbations (e.g. atmospheric loading and its mediation by the oceans) or non-linear effects in ocean tides that imply crustal loading require an explicitly time-dependent approach, connected with a substantially heavier work load in the prediction stage. Independent observations, preferably with superconducting gravimeters installed at the sites, of these perturbations will become more and more important as the precision limits of space techniques for geodynamics are pushed forward.

ACKNOWLEDGMENTS

My sincere thanks address the staff of the VLBI group at Bonn university, especially Professor J. Campbell, H. Schuh, A. Nothnagel, J. Vierbuchen, and L. Moehlmann for providing opportunity to run and study the CALC/SOLVE software, and for invaluable suggestions and assistance. I also wish to thank Prof. B. O. Rönnäng, D. D. McCarthy, D. Robertson, D. C. Agnew, and J. W. Ryan for discussions and encouragement. A. Zimmermann at Bonn has kindly provided the potential development of Büllesfeld. R. A. Flather, IOS Bidston, UK (now Proudman Laboratory) has contributed his North East Atlantic model, E. W. Schwiderski and Ulrike Seiler their global ocean models. I thank Rongjiang Wang for valuable discussions. Gabriele Marquart has helped to clean the manuscript from thoughts going astray. The studies were supported by the Natural Science Research Council of Sweden under grant number G-GU 4770.

REFERENCES

Agnew, D. C., 1983. Conservation of mass in tidal loading computations, *Geophys. J. R. astr. Soc.*, **72,** 321–325.

Aki, K. & Richards, P. G., 1980. *Quantitative Seismology, Theory and Methods,* vol. I, Freeman, San Francisco.

Baker, T. F., 1985. Methods of tidal loading computation, *Bull. d'Inform. Marées Terr.*, **94,** 6365–6373.

Baker, T. F. & Alcock, G. A., 1983. Time variation of ocean tides, in *Proc. Ninth Int. Symp. Earth Tides,* pp. 341–348, ed. Kuo, J. T., Schweizerbart, Stuttgart.

Baker, T. F., Edge, R. J. & Jeffries, G., 1989. European tidal gravity: An improved agreement between observations and models, *Geophys. Res. Lett.*, **16,** 1109–1112.

Brosche, P., Seiler, U., Sündermann, J. & Wünsch, J., 1989. Periodic changes in Earth's rotation due to oceanic tides, *Astr. Astrophys.*, **220,** 318–320.

Büllesfeld, F.-J., 1985. Ein Beitrag zur harmonischen Darstellung des gezeitenerzeugenden Potentials, *Dt. Geod. Komm., Reihe C,* **314,** Bayer. Akad. Wiss., München.

Büllesfeld, F.-J. & Schuh, H., 1986. New harmonic development of the tide-generating potential ETMB-85 with application on VLBI data analysis, in *Proc. Tenth Int. Symp. Earth Tides,* pp. 933–942, ed. Vieira, R., Cons. Sup. Invest. Cient., Madrid.

Carter, W. E. & Robertson, D. S., 1985. High-frequency variations in the rotation of the earth, *IEEE Geosci. Remote Sensing,* **GE-23,** 369–372.

Carter, W. E., Robertson, D. S. & MacKay, J. R., 1985. Geodetic radio interferometric surveying: Applications and results, *J. geophys. Res.*, **90**(B6), 4577–4588.

Cartwright, D. E. & Tayler, R. S., 1971. New computations of the tide-generating potential, *Geophys. J. R. astr. Soc.*, **23,** 45–74.

Cartwright, D. E. & Edden, A. C., 1973. Corrected tables of tidal harmonics, *Geophys. J. R. astr. Soc.*, **33,** 253–264.

Cazenave, A., 1982. Tidal friction parameters from satellite observations, in *Tidal Friction and the Earth's Rotation II,* pp. 4–18, eds Brosche, P. & Sündermann, J., Springer, Berlin.

Coates, R. J., Frey, H., Mead, G. D. & Bosworth, J. M., 1985. Space-age geodesy: The NASA Crustal Dynamics Project, *IEEE Trans. Geosci. Remote Sensing,* **GE-23,** 360–368.

Dermanis, A. & Grafarend, E., 1981. Estimability analysis of geodetic, astrometric and geodynamical quantities in very long baseline interferometry, *Geophys. J. R. astr. Soc.*, **64,** 31–56.

Dickey, J. O. & Eubanks, T. M., 1985. Earth rotation and polar motion: Measurements and implications, *IEEE Geosci. Remote Sensing,* **GE-23,** 373–384.

Dziewonski, A. M. & Anderson, D. L., 1981. Preliminary reference earth models, *Phys. Earth planet. Inter.*, **25,** 297–356.

Dehant, V., 1987. Tidal parameters for an inelastic earth, *Phys. Earth planet. Inter.*, **49,** 97–116.

Dehant, V. & Zschau, J., 1989. The effect of mantle inelasticity on tidal gravity: A comparison between the spherical and the elliptical Earth model, *Geophys. J.*, **97,** 549–556.

Fanselow, J. L. & Sovers, O. J., 1985. Observation model and parameters partials for the JPL VLBI parameter estimation software "MASTERFIT-V2.0", *JPL Public.*, 83-39 Rev.1, Pasadena, CA.

Farrell, W. E., 1972. Deformation of the earth by surface loads, *Rev. Geophys. Space Phys.*, **10,** 761–797.

Flather, R. A., 1981. Results from a model of the North East Atlantic Ocean relating to the Norwegian Coastal Current, in *The Norwegian Coastal Current, Proc. Norw. Current Symp.,* vol. II, pp. 427–458, eds Sætre, R. & Mork, M., University of Bergen.

Francis, O. & Dehant, V., 1987. Recomputation of the Green's functions for tidal loading estimations, *Bull. d'Inform. Marées Terr.*, **100,** 6962–6986.

Francis, O. & Mazzega, P., 1990. Global charts of ocean tide loading effects, *J. geophys. Res.*, **95**(C7), 11 411–11 424.

Friedrich, J. & Zimmermann, A., 1989. Report on the work of the Subgroup on Tide Generating Potential Investigations at the Institute for Theoretic Geodesy Bonn, *Bull. d'Inform. Marées Terr.*, **104,** 7330–7337.

Goad, C. C., 1980. Gravimetric tidal loading computed from integrated Green's functions, *J. geophys. Res.*, **85**(B5), 2679–2683.

Groten, E. & Brennecke, J., 1973. Global interaction between earth and sea tides, *J. geophys. Res.*, **78,** 8519–8526.

Gwinn, C. R., Herring, T. A. & Shapiro, I. I., 1986. Geodesy by radio interferometry: Studies of the forced nutations of the earth. 2. Interpretation, *J. geophys. Res.*, **91**(B5), 4755–4765.

Herring, T. A., 1986. Very Long Baseline Interferometry and its contributions to geodynamics, in *Space Geodesy and Geodynamics,* pp. 169–196, eds Anderson, A. J. & Cazenave, A., Academic Press, London.

Herring, T. A. *et al.*, 1983. Determination of tidal parameters from VLBI observations, in *Proc. Ninth Int. Symp. Earth Tides,* pp. 205–214, ed. Kuo, J. T., Schweizerbart, Stuttgart.

Herring, T. A., Gwinn, C. R. & Shapiro, I. I., 1986a. Geodesy by radio interferometry: Studies of the forced nutations of the earth. 1. Data analysis, *J. geophys. Res.*, **91**(B5), 4745–4754.

Herring, T. A., Gwinn, C. R. & Shapiro, I. I., 1986b. Correction to 'Geodesy by radio interferometry: Studies of the forced nutations of the earth. 1. Data analysis', *J. geophys. Res.*, **91**(B14), 14 165.

Herring, T. A., Davis, J. L. & Shapiro, I. I., 1990. Geodesy by radio interferometry: The application of Kalman filtering to the analysis of VLBI data, *J. geophys. Res.*, in press.

Herring, T. A., Davis, J. L. & Shapiro, I. I., 1990. Geodesy by radio interferometry: The application of Kalman filtering to the analysis of VLBI data, *J. geophys. Res.*, **95,** 12 561–12 581.

Hinderer, J. & Legros, H., 1989. Elasto-gravitational deformation, relative gravity changes and earth dynamics, *Geophys. J.*, **97,** 481–496.

Hsu, H. T., 1987. Error estimation of gravity loading correction, *Bull. d'Inform. Marées Terr.*, **99,** 6880–6896.

Jentzsch, G., 1985. The influence of the grid structure on the results of loading calculations, *Bull. d'Inform. Marées Terr.*, **94,** 6382–6368.

Kuo, J. T., Chu, Y. H. & Chen, N. M., 1986. Time-domain finite element modeling of the global ocean tides, in *Proc. Tenth Int. Symp. Earth Tides,* pp. 559–586, ed. Vieira, R., Cons. Sup. Invest. Cient., Madrid.

Ma, Ch., 1978. Very Long Baseline Interferometry applied to Polar Motion, Relativity and Geodesy, *PhD thesis,* NASA/GSFC Technical Memorandum, 79582.

Malone, F. D. & Kuo, J. T., 1981. Semi-implicit finite element methods applied to the shallow water equations, *J. geophys. res.*, **86,** C5, 4029–4040.

McCarthy, D. D. (ed.), 1989. IERS Standards (1989), *IERS Technical Note 3,* Observatoire de Paris.

Melbourne, W., 1983. Project MERIT standards, *US Naval Obs. Circ.*, vol. 167, US Naval Obs., Washington, DC.

Melchior, P., 1978. *The Tides of the Planet Earth,* Pergamon Press, Oxford.

Merriam, J. B., 1986. Transverse stress Green's functions, *J. geophys. Res.*, **91**(B14), 13 903–13 913.

Neuberg, J., Hinderer, J. & Zürn, W., 1987. Stacking gravity tide observations in central Europe for the retrieval of the complex eigenfrequency of the nearly diurnal free-wobble, *Geophys. J. R. astr. Soc.*, **91,** 853–868.

Pagiatakis, S. D., 1990. The response of a realistic earth to ocean tide loading, *Geophys. J. Int.*, **103,** 541–560.

Rabbel, W., 1982. Verformung der Erde unter atmosphärischen Auflasten, *Dipl. thesis,* Mat.-Nat. Fak., University of Kiel.

Scherneck, H.-G., 1983. Crustal loading affecting VLBI sites, *Dept. Geodesy Rep.*, vol. 20, Uppsala University.

Scherneck, H.-G., 1987. Studies of ocean loading tides at Onsala by tidal gravimetry, in *Proc. 5'th Work. Meet. Europ. VLBI f. Geod. Astr., Mitt. geod. Inst.*, vol. 71, pp. 115–133, eds Campbell, J. & Schun, H., University of Bonn.

Scherneck, H.-G., 1989. Propagation of random ocean tide model errors into computed ocean loading effects, *Bull. d'Inform. Marées Terr.*, **105,** 7482–7484.

Scherneck, H.-G., 1990. Loading Green's functions for a continental shield with a Q-structure for the mantle and density constraints from the Geoid, *Bull. d'Inform. Marées Terr.*, **108,** 7775–7792.

Scherneck, H.-G., 1990a. Regional ocean tide modelling, in *Proc. Eleventh Int. Symp. Earth Tides,* in press.

Schuh, H., 1987. Die Radiointerferometrie auf langen Basen zur Bestimmung von Punktverschiebungen und Erdrotationsparametern, *Dt. Geod. Komm., Reihe C,* vol. 328, Bayer. Akad. Wiss., München.

Schuh, H., 1989. Earth rotation parameters determined by VLBI within project IRIS, *IEEE Trans. Instr. Meas.*, **38,** 676–679.

Schuh, H. & Möhlmann, L., 1989. Ocean loading station displacements observed by VLBI, *Geophys. Res. Lett.*, **16,** 1105–1108.

Schüller, K., 1976. Ein Beitrag zur Auswertung von Erdgezeitenregistrierungen, *Dt. Geod. Komm. Reihe C,* vol. 227, Bayer. Akad. Wiss., München.

Schüller, K., 1986. Simultaneous tidal and multi-channel input analysis as implemented in the HYCON-Method, in *Proc. Tenth Int. Symp. Earth Tides,* pp. 515–520, ed. Vieira, R., Cons. Sup. Invest. Cient., Madrid.

Schwiderski, E. W., 1980a. Ocean tides, part I: Global ocean tidal equations, *Mar. Geod.*, **3,** 161–217.

Schwiderski, E. W., 1980b. Ocean tides, part II: A hydrodynamical interpolation model, *Mar. Geod.*, **3,** 219–255.

Schwiderski, E. W., 1980c. On charting global ocean tides, *Rev. Geophys. Space Phys.*, **18,** 243–268.

Schwiderski, E. W., 1981a. Global ocean tides, part IV: The diurnal luni-solar declination tide (K_1), atlas of tidal charts and maps, *NSWC TR,* vol. 81-142, Naval Surface Weapons Center, Dahlgren, VA.

Schwiderski, E. W., 1981b. Global ocean tides, part V: The diurnal principal lunar tide (O_1), atlas of tidal charts and maps, *NSWC TR,* vol. 81-142, Naval Surface Weapons Center, Dahlgren, VA.

Schwiderski, E. W., 1981c. Global ocean tides, part VII: The diurnal principal solar tide (P_1), atlas of tidal charts and maps, *NSWC TR,* vol. 81-142, Naval Surface Weapons Center, Dahlgren, VA.

Seiler, U., 1989. An investigation to the tides of the world ocean and their instantaneous angular momentum budgets, Mitt. Inst. Meereskunde, vol. 29, University of Hamburg.

Sovers, O. J., Thomas, J. B., Fanselow, J. L., O'Cohen, E. J., Purcell, G. H., Rogstad, D. H., Skjerve, L. J. & Spitzmesser, D. J., 1981. Radio interferometric determination of intercontinental baselines and earth orientation parameters utilizing Deep Space Network antennas: 1971 to 1980, *J. geophys. Res.*, **89**(B9), 7597–7607.

Tamura, Y., 1987. A harmonic development of the tide generating potential, *Bull. d'Inform. Marées Terr.*, **99,** 6813–6855.

Van Dam, T. M. & Wahr, J. M., 1987. Displacements of the earth's surface due to atmospheric loading: Effects on gravity and baseline measurements, *J. geophys. Res.*, **92**(B2), 1281–1286.

Wahr, J. M., 1981. Body tides on an elliptical, rotating, elastic and oceanless earth, *Geophys. J. R. astr. Soc.*, **64,** 677–704.

Wahr, J. M. & Sasao, T., 1981. A diurnal resonance in the ocean tide and in the earth's load response due to the resonant free 'core nutation', *Geophys. J. R. astr. Soc.*, **64,** 747–766.

Wahr, J. M. & Bergen, Z., 1986. The effects of mantle anelasticity on nutations, earth tides, and tidal variations in rotation rate, *Geophys. J. R. astr. Soc.*, **87,** 633–668.

Wahr, J. M. & de Vries, D., 1989. The possibility of lateral structure inside the core and its implications for nutation and earth tide observations, *Geophys. J. Int.*, **99,** 511–520.

Wang, R., 1986. Das viskoelastische Verhalten der Erde auf langfristige Gezeitenterme, *Dipl. thesis,* Mat.-Nat. Fak. Univ. Kiel.

Wenzel, H.-G. & Zürn, W., 1990. Errors of the Cartwright–Tayler–Edden 1973 tidal potential displayed by gravimetric earth tide observations at BFO Schiltach, *Bull. d'Inform. Marées Terr.*, **107,** 7559–7574.

Woodworth, P. L., 1985. Accuracy of existing ocean tide models, in *Proc. Conf. Use Satellite Data in Climate Models, Alpbach, Austria,* ESA-SP-244, 95–98.

Xi Qin Wen, 1987. A new complete development of the tide generating potential for the epoch J 2000.0, *Bull. d'Inform. Marées Terr.*, **99,** 6813–6855.

Yoder, C. F., Williams, J. G. & Parke, M. E., 1981. Tidal variations of Earth rotation, *J. geophys. Res.*, **86,** 881–891.

Zschau, J., 1986. Tidal friction in the solid earth: Constraints from the Chandler Wobble period, in *Space Geodesy and Geodynamics,* pp. 315–344, eds Anderson, A. J. & Cazenave, A., Academic Press, London.

Zschau, J. & Wang, R., 1986. Imperfect elasticity in the earth's mantle: Implications for earth tides and long period

deformation, in *Proc. Tenth Int. Symp. Earth Tides*, pp. 379–384, ed. Vieira, R., Cons. Sup. Invest. Cient., Madrid.

APPENDIX A

A1 Harmonic tide potential developments

Given is a set of coefficients for partial tide j, $1 \le j \le N$:

n_j	—spherical harmonic degree,
$q_j = (q_{1j}, \ldots, q_{7j})^T$	—argument numbers,
$m_j = q_{1j}$	—spherical harmonic order,
H_j	—amplitude coefficient.

The amplitude coefficients are usually scaled with respect to Doodson's constant and the 'geodetic coefficients' which are Doodson's version of spherical harmonics.

Given also is a scheme to compute the astronomical arguments (τ, s, h, p, N, p_s) (*cf.* Melchior 1978) using a polynomial in Dynamical Time (DT) counted from a given initial epoch:

$$P(DT) = \sum p_k DT^k = (\tau, s, h, p, N, p_s, \pi/2)^T,$$

$$p_0 = (0, p_{21}, \ldots, p_{61}, \pi/2)^T,$$

$$p_1 = (0, p_{22}, \ldots, p_{62}, 0)^T,$$

$$\vdots$$

$$p_k = (0, p_{2k}, \ldots, p_{6k}, 0)^T.$$

Universal time (UT ≅ UTC with sufficient accuracy) is required for the argument τ of the mean lunar day

$$\tau = UT\Omega_{MSD} + h - s,$$

$$\Omega_{MSD} = 2\pi/86400 \text{ rad s}^{-1} \quad \text{(mean solar day)}.$$

Table A1. The coefficients to be used with the Büllesfeld (1985) development of the tide potential (coefficients H_j) to conform with the conventions used in this report (amplitudes Ψ_j). Normal gravity at the equator as given by Wahr (1981, g_e = 9.798529 N kg^{-1}) is compulsory in order to remain consistent with the solid earth tide model. The w_{nm}'s renormalize Doodson's geodetic coefficients. The ρ_n's are due to Büllesfeld as well as adopted parameters on the right-hand side of:

$g_e \Psi_j = D\,(r_e/r_0)^n\, H_j/(g\rho_n w_{nm})$, $n=n_j$, $m=m_j$

r_e - equatorial radius
r_0 - mean earth radius
D - Doodson's constant $= (3/4)\, GM_{\mathbb{C}}(r_0^2/r_e^3)\sin^3\Pi_e$
Π_e - lunar equatorial parallax

n	m	w_{nm}	ρ_n
2	0	-1	1
2	1	3/2	
2	2	3	
3	0	-1	$\frac{3}{2}\cdot 1.001117$
3	1	$-8/\sqrt{15}$	
3	2	$10/\sqrt{3}$	
3	3	15	
4	0	1	$2\cdot 1.002235$
4	1	1.056026...	
4	2	-135/14	
4	3	$315\cdot\sqrt{3}/16$	
4	4	105	

$$w_{41} = \frac{5}{448}\sqrt{6\,(6\,729 + 131\sqrt{889})}$$

Table A2. The parameter for use with equations (2.4, 2.5, 2.6) associated with the effects of ellipticity and core resonance. All values are based on the Wahr (1981) theory, except [1] Farrell (1972); [2] Neuberg *et al.* (1987); [3] Dehant (1987); [4] Herring *et al.* (1986a); [5] Seiler (1989); [6] Wahr & Bergen (1986); [7] Wahr & Sasao (1981); [8] Schwiderski (1980a, b, c).

Coupling and scaling coefficients		y 0.001	H 0.6030	L 0.0841
n	m	z_m	l_m^+	w_m^+	$\beta_{nm}^{(h)}$	$\beta_{nm}^{(l)}$
2	0	0.0140	-0.0027	0.0	1.005	1.012
2	1	0.0139	-0.0014	0.0	1	1
2	1	$\tilde{z}$:-0.0720	$\tilde{l}^+$:0.0110	$\tilde{w}^+$:-0.0044		
2	2	0.0140	-0.00035	0.00053	1.010	0.998
3	m	-	-	-	0.471 [1]	0.167 [1]
4	m	-	-	-	0.285 [1]	0.118 [1]

Core resonance strength coefficients

$S_{bt}^{(h)}$	$S_{bt}^{(l)}$
$4.1\cdot 10^{-9}$	$-0.9\cdot 10^{-9}$
$(3.9+0.07i)\cdot 10^{-9}$ [6]	$(-0.93+0.01i)\cdot 10^{-9}$ [6]
$S_{at}^{(h)}$	$S_{at}^{(l)}$
$(12.8+8.0i)\cdot 10^{-6}$ [5]	$-(2.9+1.8i)\cdot 10^{-6}$ [5]
$(10.6+10.6i)\cdot 10^{-6}$ [8]	$-(2.4+2.4i)\cdot 10^{-6}$ [8]
$S_{LL}^{(h)}$	$S_{LL}^{(l)}$
$-2.88\cdot 10^{-4}$ [7]	$9.16\cdot 10^{-5}$ [7]

Core resonance frequency coefficients

$\frac{\Omega}{\omega_{NDR}-\Omega}$	434.2 [2]	434.6 [4]	observation
	460.5	459 [3]	461.6...467.3 [6] theory
Q_{NDR}	2 760 [2]		

Table A3. Ocean tides spherical harmonic coefficients, significant for liquid core resonance excitation. The leftmost column specifies the potential coefficient of the astronomical tide. Phases are with respect to the associated solid earth tide at zero meridian. [1] North Atlantic model of Flather (1981) included. [2] Amplitude adjusted for liquid core effect on tide generating potential.

Tide	Ocean tide model: Schwiderski (1981)		Seiler (1989)	
$g\Psi_j$ [$m^2 s^{-2}$]	C^+_{21} [m]	ε^+_{21} [°]	C^+_{21} [m]	ε^+_{21} [°]
O_1	0.0242	-46.3	0.0296	-51.6
0.661504	0.0245	-45.8 [1]		
P_1	0.0090	-46.1	0.0101	-61.8 [2]
0.307778				
K_1	0.0281	-44.9	0.0283	-57.8 [2]
0.930445	0.0284	-45.7 [1]		

Table A4. Parameters of the spectral model for attenuation due to anelasticity, adopted or derived from Wang (1986).

Phase exponent for $\omega > \omega_0$ / 18.6	$p^{(h)} = -0.2218$
	$p^{(l)} = -0.2945$
Love numbers at the scaling frequency ω_0 = 1 cyc/a	$h_2(\omega_0) = 0.628 \cdot \exp\{ -i\ 0.733° \}$
	$l_2(\omega_0) = 0.094 \cdot \exp\{ -i\ 3.303° \}$
at $\omega = M_f$	$h_2(M_f) = 0.616 - 3.73 \cdot 10^{-3} i$
	$l_2(M_f) = 0.089 - 1.70 \cdot 10^{-3} i$
Attenuation factors at spectral pole	$A_h = 2.753$
	$A_l = 2.005$
Calibration	$v^{(h)}_{cal} = 1.025$
$V(\omega) = v_{cal}\eta(\omega;\ \omega_{ref}=M_f)$	$v^{(l)}_{cal} = 1.075$

Usually, tables of p_{rk} specify degrees per (Julian century)$^{r-1}$. Tide phase χ_j at epoch T_0 is computed from

$$\chi_j = q_j P[DT(T_0)]$$

and frequency ω_j from

$$\frac{d\chi_j}{dUTC} \cong \frac{d\chi_j}{dDT} = q_j \sum kp_k DT^{k-1} + m_j\left[\Omega_{MSD} + \frac{d(h-s)}{dDT}\right] = \omega_j,$$

$$\omega_j t \cong \omega_j[TAI(t) - TAI(T_0)]$$
$$\cong \omega_j[UTC(t) - UTC(T_0) + DUT(t, T_0)],$$

with sufficient accuracy.

A2 Calibration of the viscoelastic relaxation model

Transformation of Dehant's value for $|h(M_f)|$ to the equatorial reference system and adjusting for the factorization of (2.4) yields an effective relaxation of 1.025 for $|h_{21}|$ with respect to the O_1 frequency. The calibration condition for relaxation function $V_2^{(h)}$ is

$$H\,|V_2^{(h)}(M_f|\,\beta_{20}^{(h)}(1-y) = |h_0^R + ih_0^I - (\tfrac{9}{4}h'_+ + 2h'_-)/\sqrt{5}| \quad \text{at } M_f, \tag{2.7}$$

where the notation on the right-hand side refers to Dehant (1987). The internal relations of the elastic response are maintained by β_{20}, and H scales the response within the total bandwidth.

APPENDIX B

Ocean loading coefficients are given in Table B1. The computations adopted in the case of:

(1) stations closer than 200 km to a coast: refined coastlines and reduced surface elements (typically 0.2° width) in a region around the site (typically 500 km radius);

(2) stations on massive shields: the Green's functions of Scherneck (1990);

(3) stations in Europe: Flather's (1981) models for M_2, S_2, K_1 and O_1;

(4) stations near a narrow continental margin or on oceanic islands: oceanic Green's functions from Farrell (1972).

In all other cases, Schwiderski's ocean tides and Farrell's Green's functions for continental structure have been used.

Tide mass conservation was imposed in all cases, using a homogeneous co-oscillating layer. However, transformation of tide height into tide mass at coasts was not carried out because of the lack of location data for the tide gauges employed in Schwiderski's models (the most frequent case is that tide values at coasts are from tide gauges, so that the correction would actually make sense).

Table B1. Ocean loading coefficients.

COLUMN ORDER: M_2 S_2 N_2 K_2 K_1 O_1 P_1 Q_1 M_f M_f S_{sa}

ROW ORDER:
Site: name, longitude, latitude
Amplitudes (10^{-5} m)
  RADIAL / TANGENTIAL EW / TANGENTIAL NS
Phases (°)
  RADIAL / TANGENTIAL EW / TANGENTIAL NS

Tangential displacements are positive towards west and south.

ONSALA	11. 9263	57. 3947								
384	91	84	19	224	120	71	3	84	63	17
124	34	31	9	42	41	15	6	18	10	18
58	27	21	8	32	17	9	4	7	1	18
-56.0	-46.1	-90.7	-34.4	-44.5	-123.2	-49.6	178.4	14.9	37.3	3.4
75.4	97.6	40.8	94.8	119.0	25.4	98.7	-14.1	-177.0	-126.7	-177.0
84.2	131.3	77.7	103.9	17.2	-55.0	25.2	-165.0	173.3	121.8	106.4

Table B1. (*continued*)

WETTZELL		12. 8774		49. 1437						
494	143	104	34	182	77	56	4	35	20	5
182	49	41	15	31	21	12	4	7	4	10
46	17	8	6	31	7	8	2	7	4	12
-69.0	-38.1	-86.9	-35.9	-58.3	-101.1	-59.7	-112.2	5.8	0.7	-61.4
65.0	100.3	42.2	96.3	105.3	20.5	87.9	-7.6	161.2	70.2	157.6
-27.6	23.2	-7.7	37.5	24.9	-64.8	23.6	164.8	-151.5	134.3	121.4
MADRID		-4. 2480		40. 4300						
1357	452	288	120	230	31	70	21	34	21	21
311	114	83	39	23	12	13	7	7	12	16
307	113	60	30	31	26	9	9	9	5	8
-87.4	-61.7	106.8	-65.3	-70.9	-147.4	-72.9	58.0	-30.6	-110.0	-24.5
-50.2	-20.0	38.6	82.9	-85.3	-165.1	59.6	-78.3	114.7	53.5	118.7
-56.5	-18.1	-77.4	-19.2	-28.9	-156.3	-39.2	155.1	-98.6	-177.0	174.9
RICHMOND		-80. 3847		25. 6128						
871	250	144	62	192	135	63	34	47	23	133
401	70	91	20	72	75	25	16	2	2	18
234	40	61	12	30	31	11	6	5	3	10
167.2	-162.4	147.0	-168.8	17.2	26.4	14.9	36.7	148.0	144.7	-144.6
-179.0	-163.9	160.7	-166.7	43.2	40.6	44.9	36.4	1.2	-140.6	-99.1
-155.1	-88.0	176.1	-90.0	-16.8	-65.2	-3.9	-98.7	-94.5	144.1	80.2
HRAS085		-103. 9472		30. 6356						
105	153	45	44	473	320	149	64	15	11	25
117	27	26	10	200	132	62	23	5	2	24
114	50	28	15	58	32	19	9	5	4	6
-177.9	-128.1	-63.7	-111.9	32.7	18.2	30.6	11.1	-171.6	-173.1	166.3
149.9	159.8	119.8	141.1	-141.7	-158.4	-143.5	-168.1	114.2	127.9	-147.4
96.8	96.3	93.3	95.6	140.3	147.9	136.8	151.3	-146.4	-175.9	-136.4
WESTFORD		-71. 4881		142. 6163						
1024	278	221	78	400	269	129	57	37	21	27
421	96	95	26	36	22	10	4	9	4	23
225	62	48	17	30	37	9	11	10	8	5
-175.0	-151.1	168.0	-157.8	-5.0	-3.9	-3.6	-1.8	13.7	66.6	-176.3
-144.8	-123.1	-169.4	-129.7	-11.4	23.6	-16.5	31.8	0.7	165.0	-76.2
-17.6	21.3	-26.6	16.0	-177.5	-147.7	-173.2	-165.0	-151.4	-144.7	-6.4
ALASKA NO		-147. 4975		64. 9775						
779	324	112	82	501	348	161	64	72	44	12
63	25	17	9	95	71	30	17	4	0	17
332	133	58	36	202	127	64	23	13	12	21
101.4	139.7	87.1	135.6	96.5	88.2	95.9	81.7	17.8	20.6	-117.6
103.0	-81.6	56.1	-63.5	-1.6	-36.2	-3.6	-41.0	-179.4	131.4	147.3
-90.1	-49.3	104.5	-50.5	-101.1	-112.1	-101.3	-116.6	147.0	-136.7	-132.0
OVRO130		-118. 2827		37. 2303						
276	102	97	31	1000	629	310	118	12	3	25
238	79	41	20	295	188	89	32	7	4	25
319	127	71	39	156	94	48	20	6	4	14
38.5	-143.5	-33.2	-97.2	47.1	32.7	46.5	24.4	-45.0	99.2	105.6
-125.7	-75.0	-153.8	-78.8	-126.1	-139.4	-125.9	-143.3	141.2	113.5	-169.2
97.7	111.2	79.6	108.1	179.6	167.4	178.1	158.1	-162.1	177.3	-119.8
KASHIMA		140. 6627		35. 9529						
948	486	137	136	1180	926	364	188	20	54	108
289	146	36	38	215	176	70	38	6	10	33
167	68	30	22	188	141	57	26	4	13	10
50.7	75.1	63.1	77.9	-138.7	-157.9	-138.9	-163.2	-11.2	42.5	103.5
5.6	41.0	5.8	46.9	-166.5	172.3	-165.3	169.5	-7.1	10.3	48.6
-70.4	-56.5	-74.4	-51.2	93.6	70.4	95.5	54.9	169.6	-158.8	-117.9
MOJAVE		-116. 8876		35. 3305						
202	146	112	54	986	623	307	117	11	6	45
181	50	31	11	297	187	91	32	8	3	27
341	138	75	43	159	97	50	21	5	2	11
-8.7	-110.7	-53.3	-86.9	44.0	29.3	43.1	20.9	-78.0	171.0	45.4
-141.7	-81.5	-176.7	-90.1	-130.1	-144.0	-130.1	-149.3	135.8	157.3	-138.7
97.1	111.5	80.0	108.4	179.5	168.0	177.8	159.2	12.3	36.3	-117.5
MARPOINT		-77. 2306		38. 3730						
919	244	169	69	330	226	108	49	15	8	37
414	90	93	26	22	15	6	4	6	3	19
85	28	11	8	16	24	5	8	8	6	6
158.0	-170.1	140.1	-173.8	-2.0	-0.6	-0.5	3.6	24.8	81.2	-179.1
-176.0	-150.1	163.9	-155.0	-27.0	43.8	-31.9	51.8	-2.6	-170.9	-87.3
-42.7	9.4	-52.6	5.0	-168.8	-132.9	-164.0	-156.8	-135.5	-161.0	6.0
GREENBANK		-79. 8358		38. 4366						
720	205	124	57	293	200	96	43	10	3	36
354	77	79	23	14	8	4	3	4	4	17
50	22	4	6	9	17	2	6	8	6	5
153.0	-172.4	132.4	-175.4	0.2	0.4	1.7	4.5	29.0	96.5	-178.3
-174.2	-149.0	164.5	-154.1	-80.9	108.7	-90.8	90.5	-5.0	-154.7	-92.4
-58.8	14.5	-94.9	9.5	164.5	-125.1	169.3	-156.9	-135.4	-163.0	5.2
TIDBINBILLA										
951	128	204	31	276	278	103	83	14	5	48
515	182	91	49	125	73	40	14	3	15	10
116	37	19	12	147	129	50	29	6	5	17
125.7	173.0	96.0	161.2	118.6	67.0	111.9	53.9	-18.9	-73.9	-96.9
93.0	126.4	82.3	128.8	-168.6	169.1	-170.4	148.2	-105.3	73.1	134.8
7.9	70.2	-31.5	79.8	-117.0	-143.6	-117.5	-160.6	-144.8	92.7	116.0